53/6-8-93/9752

PREPARED FOR THE U.S. DEPARTMENT OF ENERGY,
UNDER CONTRACT DE-AC02-76-CHO-3073

PPPL-2900
UC-426

PPPL-2900

INVESTIGATION OF ELECTROSTATIC WAVES IN THE ION CYCLOTRON RANGE OF FREQUENCIES IN L-4 AND ACT-1

BY

M. ONO

MAY, 1993

PPPL PRINCETON PLASMA PHYSICS LABORATORY

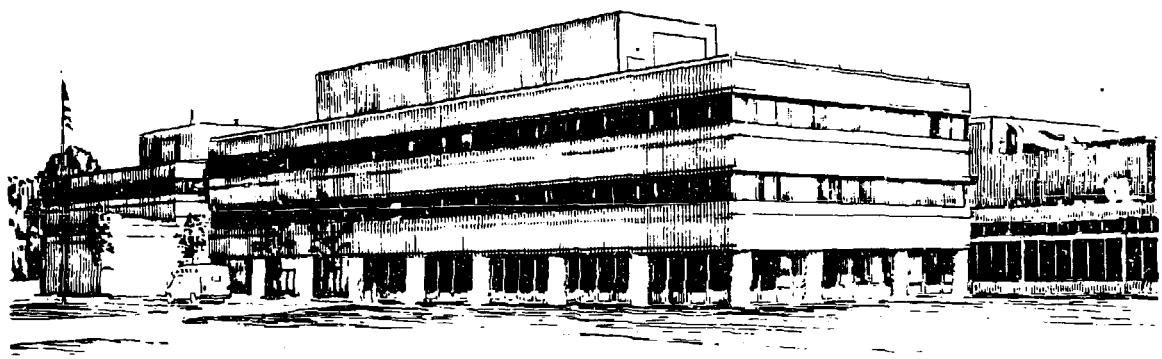

PRINCETON UNIVERSITY, PRINCETON, NEW JERSEY

INVESTIGATION OF ELECTROSTATIC WAVES IN THE ION CYCLOTRON RANGE OF FREQUENCIES IN L-4 AND ACT-1

Masayuki Ono

Princeton Plasma Physics Laboratory, Princeton University,
P.O. Box 451, Princeton, New Jersey, 08543, USA

Abstract

Electrostatic waves in the ion cyclotron range of frequencies (ICRF) were studied in the Princeton L-4 and ACT-1 (the Advanced Concept Torus-1) devices for approximately ten years, from 1975 to 1985. The investigation began in the L-4 linear device, looking for the parametric excitation of electrostatic ion cyclotron waves in multi-ion-species plasmas. In addition, this investigation verified multi-ion-species effects on the electrostatic ion cyclotron wave dispersion relation including the ion-ion hybrid resonance. Finite-Larmor-radius modification of the wave dispersion relation was also observed, even for ion temperatures of $T_i \approx 1/40$ eV (~ the room temperature!). Taking advantage of the relatively high field and long device length of L-4, the existence of the cold electrostatic ion cyclotron wave (CES ICW) was verified. This branch occurs below the ion cyclotron frequency and, in a two-ion-species plasma, shows a resonance at the ion-ion hybrid frequency.

With the arrival of the ACT-1 toroidal device, finite-Larmor-radius (FLR) waves were studied in a relatively collisionless warm-ion hydrogen plasma. Detailed investigations of ion Bernstein waves (IBW) included the verification of mode-transformation in their launching, their wave propagation characteristics, their absorption, and the resulting ion heating. This basic physics activity played a crucial role in developing a new reactor heating concept termed ion Bernstein wave heating (IBWH).

Experimental research in the lower hybrid frequency range confirmed the existence of FLR effects near the lower hybrid resonance, predicted by Stix in 1965. In a neon plasma with a carefully placed phased wave exciter, the neutralized ion Bernstein wave was observed for the first time. Using a fastwave ICRF antenna, two parasitic excitation processes for IBW -- parametric instability and density-gradient-driven excitation -- were also discovered.

In the concluding section of this paper, a possible application of externally launched electrostatic waves is suggested for helium ash removal from fusion reactor plasmas.

INTRODUCTION

Historically, research concerning waves in the ion cyclotron range of frequencies (ICRF) has focused on the electromagnetic waves, such as the ion cyclotron and fast magnetosonic waves, due to their application to plasma heating.[1] Electrostatic waves have been studied primarily to understand phenomena in the plasma edge region during high power rf heating. For example, electrostatic waves can be excited inadvertently through parametric instabilities and parasitic processes associated with high power ICRF heating. These electrostatic waves are apt to heat the plasma edge and produce an influx of impurities. Also, it was pointed out in 1975 that fast waves can undergo mode-conversion into ion Bernstein waves (IBW) near the heating layer, a process that may play a significant role in ICRF power absorption.[2] Earlier, in 1965, Stix proposed that the FLR effects could cause mode-conversion of the electron plasma wave into hot plasma modes near the lower hybrid resonance.[3] Pioneering experiments performed in this area include those on ion acoustic waves,[4] electrostatic ion cyclotron waves,[5] and pure ion Bernstein waves,[6] to name a few. However, there were many more electrostatic modes and processes that needed experimental verification. In particular, data on multi-ion-species effects were largely absent. For example, the existence of ion-ion hybrid resonance phenomena was only inferred through external measurements such as antenna loading.[7] In the area of finite-Larmor-radius modes, the experimental data were essentially limited to the Q-machine experiments. How these electrostatic waves (through linear and/or nonlinear processes) are excited by external antennas was not yet well understood in this frequency range. In the Princeton L-4 device, the study of electrostatic waves in the ion cyclotron range of frequency began in 1975 with an emphasis on parametric instability processes in multi-ion-species plasmas.[8] This work led to the observation of new parametric instability processes in the ion cyclotron range of frequencies.[9-11] At the same time, the research also produced useful information on FLR-modified electrostatic waves in multi-ion species plasmas.[9-11]

After completion of the parametric instability study, the L-4 device was found uniquely suited to verify the existence of the cold electrostatic ion cyclotron wave.[12] Then, in 1979, to examine new concepts for rf current drive[13] and for finite-ion-temperature waves,[14] the L-4 linear device was converted into the ACT-1 torus.[15] Although it is outside of the scope of the present paper, it should be noted that the initiation of current-drive research on ACT-1 has led to a very productive series of experiments starting with the first verification of the lower hybrid current drive in a toroidal plasma.[16] This work evolved into experiments on other types of current drive including fast-wave current drive,[17] helicity-injection current drive in CDX (the Current Drive Experiment performed in the ACT-1 facility),[18] and the pressure-driven-currents in CDX-U (the Current Drive Experiment - Upgrade facility replaced the ACT-1 facility

in 1990).[19] Going back to the investigation of electrostatic waves in ACT-1, using warm hydrogen plasmas, the physics of ion Bernstein waves was investigated extensively.[20-24] Emerging from this study came a promising reactor heating concept utilizing externally launched IBW.[14,25] Later experiments in ACT-1 then found long elusive plasma modes including the hot plasma waves (HPW) excited near the lower hybrid mode-conversion layer[24,26] and the well-known neutralized ion Bernstein wave.[27,28] Parasitic IBW excitation processes relevant for the ICRF heating were also examined.[29,31]

This paper intends to review the topic of electrostatic waves in the ion cyclotron range of frequencies, to summarize research work performed in L-4 and ACT-1 in this area, and to guide interested readers to the original manuscripts for more detail, many of which are Ph.D. theses. In the present paper, we first review the pertinent dispersion relations. Then mode conversion and mode transformation process (applicable to electrostatic waves) are discussed. Experimental parameters important for the L-4 and ACT-1 experiments are described. We next present some experimental highlights, starting with the laboratory determination of the dispersion relation for various waves, mode-transformation and mode-conversion processes, IBW heating experiments, and ICRF-relevant parasitic IBW excitation processes. Finally, we suggest using externally launched IBW and/or CES ICW to remove helium ash from fusion-reactor plasmas.

ELECTROSTATIC WAVE DISPERSION RELATION

The quasi-electrostatic wave dispersion relation in the ion cyclotron range of frequency including the finite-Larmor-radius effect can be written as,[1]

$$n_\perp^2 K_{xx} + (n_\parallel^2 - K_{xx})K_{zz} = 0 . \qquad (1)$$

where K_{xx}, and K_{zz} are elements of the plasma dielectric tensor which in a non-drifting Maxwellian plasma can be expressed as

$$K_{xx} = 1 + \frac{\omega_{pe}^2}{\Omega_e^2} + \sum_i \frac{\omega_{pi}^2}{\omega - k_\parallel V_i} \frac{e^{-b_i}}{b_i} \sum_{n=1}^{\infty} n^2 I_n (Z_n + Z_{-n}) \qquad (2)$$

$$K_{zz} = 1 + \frac{2\omega_{pe}^2}{k_\parallel^2 V_e^2} (1 + \xi_{e0} Z_0) \qquad (3)$$

where the summation i is over ion species, n is the harmonic number, Z_n is the plasma dispersion function[32] of argument $\xi_{\sigma n} \equiv (\omega - n\,\Omega_\sigma) / k_\parallel V_\sigma$, σ denotes species, $V_\sigma \equiv$

$(T_\sigma/m_\sigma)^{1/2}$ and I_n is the modified Bessel function with argument $b_i \equiv k_\perp^2 T_i / m_i \Omega_i^2$. Here $n_\perp \equiv ck_\perp/\omega$ and $n_\parallel \equiv ck_\parallel/\omega$. The finite-Larmor-radius (FLR) wave formalism was established in 1960's by Bernstein.[33] The generalized dispersion relation was later given in Stix.[1]

To illuminate the multi-ion species and FLR effects, it is instructive to expand terms in Eq.(2) for small $b_i \equiv (1/2)\langle k_\perp \rho_i \rangle^2$, a particularly good approximation for $\omega \approx 2\Omega_i$. Retaining the leading order terms in b_i and assuming large ξ_{in}, one obtains a quadratic equation in $k_\perp^2$ as

$$a\, k_\perp^4 + b\, k_\perp^2 - c = 0 \tag{4}$$

where

$$a = \sum_i 3 \frac{\omega_{pi}^2 (T_i / m_i)}{(4\Omega_i^2 - \omega^2)(\omega^2 - \Omega_i^2)}$$

$$b = 1 - \sum_i \frac{\omega_{pi}^2}{(\omega^2 - \Omega_i^2)}$$

$$c = k_\parallel^2 \frac{\omega_{pe}^2}{\omega^2} \qquad \text{for } \frac{\omega}{k_\parallel} > V_{Te} \text{ or}$$

$$= -2\frac{\omega_{pe}^2}{V_{Te}^2}. \qquad \text{for } \frac{\omega}{k_\parallel} < V_{Te}$$

The coefficients a, b, and c represent the finite-Larmor-radius (ion thermal) correction term, the cold ion term, and the cold (or hot) electron term, respectively. For multi-ion-species plasma, we assume species 1 to have the highest ion cyclotron frequency. In an axisymmetric system such as tokamak, one can often assume $n_\parallel$ to be a constant or only slowly varying. We shall therefore examine here the wave dispersion relation with the $k_\perp$ as a variable. The solution for Eq. (4) is

$$k_\perp^2 = \frac{-b \pm \sqrt{b^2 + 4ac}}{2a} \tag{5}$$

We shall now consider various limiting cases of Eq. (5).

A. Waves in cold electron plasmas ($\omega / k_\parallel > V_{Te}$).

For cold electrons, c is positive. There are then four main propagating modes depending on the signs of b and a. Examining these four limiting cases:

1. Electron plasma wave or EPW ($\omega > \omega_{pi}$)

In a sufficiently low density plasma ($\omega > \omega_{pi}$), b is positive and a is small. Then, $k_\perp^2 \approx c/b$ or

$$k_\perp^2 \left(1 - \sum_i \frac{\omega_{pi}^2}{(\omega^2 - \Omega_i^2)}\right) - k_\parallel^2 \left(\frac{\omega_{pe}^2}{\omega^2}\right) = 0 \qquad (6)$$

which is the well-known electrostatic lower-hybrid-wave dispersion relation. The wave exhibits a resonance ($k_\perp \rightarrow \infty$) at the lower hybrid frequency, $\omega \approx \omega_{pi}$. For intermediate densities such that $\omega_{pe}^2 >> \omega^2 >> \omega_{pi}^2, \Omega_i^2$, the dispersion relation becomes particularly simple, $\omega \approx (k_\parallel / k_\perp)\omega_{pe}$. It then follows that $\partial\omega/\partial k_\perp \approx - \omega/k_\perp$; the wave is a backward propagating wave (the wave phase velocity points in the direction opposite to the wave group velocity). It also exhibits "resonance cone" behavior[34,35] [the direction of the group velocity is the same for all wave numbers, i.e., $v_{g\perp} / v_{g\parallel} = (\partial\omega/\partial k_\perp)/(\partial\omega/\partial k_\parallel) \approx - \omega/\omega_{pe}$]. Measurement of the resonance-cone angle, $\theta \equiv \tan^{-1} [v_{g\perp}/v_{g\parallel}]$, which depends only on the electron density for a given wave, often gives a convenient way of determining the plasma density in a laboratory plasma. The understanding of the launching and propagation of electron plasma waves is highly relevant to lower-hybrid wave heating, and detailed investigations[36,37] have been carried out for that reason.

2. Ion Bernstein wave ($\omega \approx$ few Ω_i and $\omega < \omega_{pi}$)

For $\Omega_i < \omega < 2\Omega_i$, a is positive, and one can see a continuous evolution of propagating solutions ($k_\perp^2 > 0$) from the low-density electron plasma wave (EPW) regime where $b \approx 1$ (i.e., $k_\perp^2 \approx c/b \approx k_\parallel^2 \omega_{pe}^2/ \omega^2$) to the higher density ($\omega < \omega_{pi}$) ion Bernstein wave (IBW) regime for $b < 0$. In the limit of $b << 0$, one obtains $k_\perp^2 \approx |b|/a$, or for a single ion species plasma,

$$k_\perp^2 \approx (4\Omega_i^2 - \omega^2) / 3(T_i / m_i) \qquad (7)$$

where the electron term drops out entirely and the dispersion relation becomes independent of plasma density. The IBW dispersion relation exhibits a cut-off behavior

($k_\perp \rightarrow 0$) as $\omega \rightarrow 2\Omega_i$. It is also clear that the perpendicular IBW phase and group velocities are proportional to the ion thermal velocity, V_{Ti}. And again, the wave is a backward propagating wave. For a two ion species plasma, the IBW exists between the ion-ion hybrid frequency, ω_{ih}, defined as $\omega_{ih}^2 = (\omega_{p1}^2\Omega_2^2 + \omega_{p2}^2\Omega_1^2) / (\omega_{p1}^2 + \omega_{p2}^2)$ and the lower ion cyclotron frequency, Ω_2. The propagating bands are therefore $\omega > \Omega_1$ and $\omega_{ih} > \omega > \Omega_2$ Solving Eq. (1) in full, one obtains the IBW propagating branches for various harmonic frequencies. See, for example the paper by Swanson.[38] In the limit of $n_{||} \rightarrow 0$, the electron term drops from the dispersion relation altogether, leaving the "pure" ion Bernstein wave where the wave oscillation is sustained by the ion-Larmor-radius dynamics alone. In this limit the wave dispersion relation is simply $K_{xx} = 0$. J. Schmitt was able to observe this wave in a cesium plasma by using a wire exciter which was strung carefully along a magnetic field line in order to satisfy the $n_{||} = 0$ condition.[6] Typically, the IBW shows a cut-off behavior as ω approaches $n\Omega_i$ from below. Similarly, a resonant behavior appears when $n\Omega_i$ is approached from above.

3. Hot plasma waves (HPW) in the lower hybrid wave frequency range ($\omega >> \Omega_i$ and $\omega > \omega_{pi}$)

It turns out that Eq. (5) can also describe[3] FLR effects for the lower-hybrid wave ($\omega >> \Omega_i$). The term $a = -3\omega_{pi}^2 (T_i / m_i) / \omega^4$ in Eq. (5) becomes negative. The only propagating solutions are when $b \approx 1 - \omega_{pi}^2 / \omega^2$ is positive or $\omega_{pi}^2 < \omega^2$. One solution of Eq. (5) is the electron plasma wave or the lower hybrid wave. The other root describes the dispersion relation of the hot plasma wave, $k_\perp^2 \approx b / |a|$ or

$$k_\perp^2 = \frac{\omega^4 - \omega_{pi}^2 \omega^2}{3\,\omega_{pi}^2 (T_i / m_i)} \qquad (8)$$

It is easy to show that this mode is a forward propagating mode. It should be noted that this mode can also exists in the hot electron plasma since the dispersion does not depends on the electron term.

4. Cold electrostatic ion cyclotron wave, or CES ICW ($\omega < \Omega_i$ and $\omega < \omega_{pi}$)

In this regime, since $\omega < \Omega_i$, b is positive, and the solution is $k_\perp^2 \approx c/b$. The form is the same as for the EPW. The dispersion relation can then be written as

$$k_\perp^2 \;=\; \frac{k_\parallel^2\,(\omega_{pe}^2/\omega^2)}{\sum_i \omega_{pi}^2/(\Omega_i^2-\omega^2)} \qquad (9)$$

The CES ICW dispersion relation shows a cut-off behavior ($k_\perp \rightarrow 0$) as $\omega \rightarrow \Omega_i$. In a two-ion-species plasma, the wave exhibits resonance behavior ($k_\perp \rightarrow \infty$) at the ion-ion hybrid frequency[7], ω_{ih}, where the denominator of Eq. (9) vanishes. The propagating bands are $\omega < \Omega_2$ and $\omega_{ih} < \omega < \Omega_1$. One should point out that the propagation bands of the CES ICW are complementary to those of the IBW. The CES ICW is backward propagating and exhibits resonance-cone behavior.[34,35] One can show from Eq. (9) that the cone angle $\theta \equiv \tan^{-1}[v_{g\perp}/v_{g\parallel}] \approx \Sigma_i\,[\omega_{pi}/\omega_{pe}](\Omega_i^2/\omega^2 - 1)^{-1/2}$ depends only on the values of local ω/Ω_i and ion concentration Since ω/Ω_i is an accurately known quantity, measurement of the cone angle in this instance is able to provide a convenient method for determining the ion concentration.[12] Since this mode can be excited in about the same frequency band as the ion cyclotron wave (the slow wave), it may be related to the infamous Mode X observed during early ion cyclotron heating experiments carried out in the C-Stellarator with no Faraday shielding for the antenna.[39] That this mode can be easily excited by an external antenna was, in fact, demonstrated in L-4.[12]

Further analysis including the electromagnetic terms shows that CES ICW cannot penetrate beyond the Alfvén resonance. Thus it is not suitable for core plasma heating. On the other hand, it will be pointed out in the concluding section that this mode may be well suited for edge heating, or may be used for the removal of helium ash or impurity ions.

B. Waves for hot electron plasmas ($\omega / k_\parallel < V_{Te}$).

For hot electrons, c is negative and there are two well-known propagating roots in the negative b region ($\omega > \Omega_i$ and $\omega < \omega_{pi}$). Equation. (5) can then be written as

$$k_\perp^2 \;=\; \frac{|b| \pm \sqrt{b^2 - 4a|c|}}{2a} \qquad (10)$$

1. Electrostatic ion cyclotron wave ($\omega > \Omega_i$)

The negative root, $k_\perp^2 = |c|/|b|$ or

$$k_\perp^2 \approx \frac{(\omega_{pe}^2 / V_{Te}^2)}{\sum_i \omega_{pi}^2 / (\omega^2 - \Omega_i^2) - 1} \qquad (11)$$

which is the electrostatic ion cyclotron wave (ES ICW).[5] This mode is insensitive to the plasma density and the phase velocity is proportional to the ion acoustic velocity, $C_s \approx (T_e / m_i)^{1/2}$. The dispersion relation asymptotically approaches that of the ion acoustic wave for $\omega >> \Omega_i$ since the wave can be considered unmagnetized. The ES ICW dispersion relation exhibits a cut-off behavior ($k_\perp \to 0$) as $\omega \to \Omega_i$.[5] In a two-ion-species plasma, the wave exhibits a resonance behavior ($k_\perp \to \infty$) as it approaches the ion-ion hybrid frequency, ω_{ih}, and the lower hybrid frequency, $\approx \omega_{pi}$, from below.[9] The propagating bands are $\Omega_2 < \omega < \omega_{ih}$ and $\omega > \Omega_1$. As can be shown from Eq. (11), the ES ICW is a forward-propagating mode.

2. Neutralized ion Bernstein wave ($\omega > \Omega_i$)

The positive root, $k_\perp^2 \approx |b| / a \approx (4\,\Omega_i^2 - \omega^2) / 3(T_i / m_i)$ has the same dispersion relation as the ion Bernstein wave, Eq (7). However, in this case, the electrons are hot. Because their rapid movement along the field line neutralizes the plasma, this mode is termed the neutralized ion Bernstein wave. The propagating bands of the neutralized IBW are similar to those of the ES ICW. As an IBW, it is a backward-propagating mode.[27,28]

C. Mode-conversion and mode-transformation processes

At the point where the square root term of Eq.(5), $(b^2 + 4ac)$, becomes zero, the two propagating modes [the + root and - root of Eq (5)] merge. This coming together of two different types of waves [i.e., one forward (fw) and one backward (bw)] in the propagating side of the conversion point (i.e., $b^2 + 4ac > 0$) has been termed mode conversion.[3] It represents a true wave singularity in that the group velocity goes to zero at this point. As the wave numbers must match at the conversion point, $k_\perp^2 \approx -b/2a$, the wave group velocity must cross zero. Recall that the group velocities of those two waves start with opposite signs (i.e., they comprise a fw and a bw). Because of this singular behavior, the conversion efficiency is usually not 100%. The wave could be partially reflected. In some situations, the wave could tunnel to the other side if the thickness of the evanescent layer is sufficiently small. This type of problem has been studied in detail for ICRF heating.[2,40] There are also many examples of mode conversion among electrostatic waves: EPW (bw) into HPW (fw); further mode conversion of HPW (fw) into IBW (bw); and ES ICW (fw) into neutralized IBW (bw). For lower hybrid waves, the EPW can mode convert to a HPW, and the converted

HPW can again mode convert to an IBW which can then be thermalized by the plasma. This possibility of double-mode-conversion for the lower hybrid heating was first pointed out by Stix.[3]

Mode-transformation on the other hand describes a process where a plasma wave, as it propagates in a non-uniform plasma, undergoes an intact transformation into another type of wave due to a change in the plasma parameters (e.g. density or magnetic field gradient).[14,20] Mode transformation occurs when waves of similar type (two forward waves or two backward waves) are joined together. As long as the WKB condition is satisfied, the mode transformation efficiency is 100%. There is no wave singularity for this case. It is easy to verify this point since the wave number stays finite and the group velocity always retains the same sign (and stays finite). The mode stays on the same root of Eq. (5) but changes its property due to the change in the plasma parameters. Three cases of the mode transformation process among the backward waves are discussed here: 1. EPW into IBW, when b changes sign from positive to negative at the lower hybrid resonance, $\omega \approx \omega_{pi}$; 2. EPW into CES ICW has a rather fuzzy transition at $\omega \approx \omega_{pi}$ since b is always positive here; and 3. CES ICW into IBW, when b changes sign from positive to negative at $\omega = \omega_{ih}$. Although not observed experimentally (to the author's knowledge), there appears to be a mode-transformation process that connects two forward waves for $\omega >> \Omega_i$ (negative a), ES ICW and HPW at b=0. By utilizing this process, one might excite a desired wave with good efficiency by actually exciting another type of wave perhaps launched more easily by an external antenna. For IBW heating, one typically uses the EPW → IBW mode-transformation process, transforming a launched electron plasma wave into the ion Bernstein wave for which one expects better wave accessibility to the hot-dense plasma core. One can also launch CES ICW via the EPW→CES ICW mode-transformation.

A comparison of mode transformation and mode conversion is shown in Fig. 1 where the wavenumber is plotted as a function of the plasma position. Density increases going away from the antenna. The lower curve shows the mode transformation of an EPW into an IBW for $\Omega_i < \omega < 2\Omega_i$ where a is positive. One sees a continuous evolution of the refractive index ($k_\perp^2 > 0$) from the low density electron plasma wave (EPW) regime, where $b \approx 1$ (i.e., $k_\perp^2 \approx c/b$), to the higher density ($\omega < \omega_{pi}$) ion Bernstein wave (IBW) regime where $b << 0$ (i.e., $k_\perp^2 > |b|/a$). The cold plasma resonance disappears for a finite ion temperature plasma. By keeping the higher order terms, one can show that mode transformation also occurs for the waves launched at higher harmonics, provided that the ion temperature in the transformation region, near $\omega \approx \omega_{pi}$, is sufficiently high . In general, for the n-th

harmonic launching case, the higher $k_\perp \rho_i$ values require that T_i for a smooth transformation go up as $10^{(n/2-1)}$ in the transformation region.[21]

The dashed upper curve in Fig. 1 shows the mode-conversion process for $\omega >> \Omega_i$ with $a < 0$ relevant for lower hybrid heating. One can see that EPW branch connects to HPW mode at the mode-conversion point. It should be noted that near the turning point, the WKB treatment breaks down and a proper treatment of the differential wave equation is required.[3]

III. Experimental setup

A. Experimental parameters of L-4 and ACT-1

Electrostatic waves in the ion cyclotron range of frequency were studied in the L-4 linear device (1975-79) and the ACT devices (1980-1985). A brief description of the relevant plasma parameters for L-4 and ACT-1 follows.

L-4 was a steady-state linear device with a uniform magnetic field extending over approximately 230 cm. The axial magnetic field strength could rise to 4.2 kG and spatial field ripple was below 0.5 %.[11] As shown in Fig. 2, plasma was produced by a hot tungsten filament plasma source[41] located at one end of the device. Emitted electrons are mirror confined by a large number of small permanent magnets placed with alternating polarity on the wall of the filament source chamber. The emitted electrons produce plasma by ionizing the neutral background gas. However, the ionization efficiency was relatively small (since the required ionization path length was usually much longer than the device length) and the resulting plasma was only weakly ionized (≈ 1%). Typical plasma parameters used in the experiments are as follows: plasma density, $n_0 \leq 3 \times 10^{10} cm^{-3}$; electron temperature, $T_e \approx 2$ - 5 eV; ion temperature, $T_i \leq 1/10$ eV; plasma drift velocity $\leq 0.1\ c_s$; and the plasma density fluctuation, $\delta n/n \approx 1$ - 2% in the plasma center and 2 - 5 % at the edge of the plasma.

ACT-1 (Advanced Concept Torus-1) was a simple toroidal machine with major and minor radii of 59 cm and ~ 6 cm, respectively, and a plasma circumference of about 350 cm.[15] A schematic drawing is given in Fig. 3. One of the unique features of ACT-I was the excellent plasma access provided by the twenty-six 10 × 40 cm large rectangular windows. The magnetic field ripple was < 1% in the central region of the plasma and the steady-state toroidal magnetic field was typically used at 5 kG. Plasma was created by a hot tungsten filament strung in the high field region as shown in Fig. 4.[17] Emitted electrons circulate around the torus many times before being lost to the wall. The relatively long electron path length (3.7 meters times the number of transits

around the torus can often exceed 100 m) insures efficient ionization of the background neutral gases. As shown by Fig. 4, the plasma consists of a narrow vertical band with hot electrons near the filament while a diffuse lower-density plasma filled the remaining space bounded by the conducting limiter. As the diffuse plasma is free of hot electrons and is nearly Maxwellian, most of the wave propagation experiments were conducted in this region. The ∇B-drift-generated vertical currents were allowed to flow to the conducting plasma boundaries (or limiters), and in this way the equilibrium of the plasma was maintained. This type of equilibrium produced plasmas that were relatively uniform in the vertical direction. The measured radial plasma drift was small, $< 0.1\ c_s \approx 10^5$ cm/sec. Density fluctuations were typically 5 - 10%. A good stable discharge could be maintained even for gauge neutral pressure as low as 7×10^{-6} Torr, resulting in a warm-ion ($T_i \leq 2$ eV), $T_e \approx$ few eV, highly ionized ($\leq 30\%$), low collisionality hydrogen plasma with $n_e \leq 10^{11} cm^{-3}$.

In the ion cyclotron range of frequencies, it is often important to use a strong magnetic field to attain a high wave frequency (noting that $\omega \sim \Omega_i$) and avoid excessive wave dissipation processes such as ion collisions. Similarly, for cold electron modes it is important to avoid electron Landau damping. In a typical laboratory plasma, it is not always possible to investigate *cold-electron* ion cyclotron modes since the excitable wave parallel phase velocity is not large enough to avoid electron Landau damping, $\omega / k_{\parallel} = f \lambda_{\parallel} > 2 - 3\ V_{Te}$. If the plasma temperature is a few eV ($V_{Te} \approx 1 \times 10^8$ cm/sec), the wave parallel phase velocity must therefore exceed $2 - 3 \times 10^8$ cm/sec. If one assumes that it is possible to excite a wave with a well defined $\lambda_{\parallel} \approx 50$ cm (this value must be small compared to the plasma size), then the wave frequency must be at least 4 - 6 MHz. This means that the ion cyclotron frequency must be of the order of a few MHz. For hydrogen, the value is reasonable, B = 2 - 3 kG. However, the required value goes up linearly with ion mass. If one were to use a cesium plasma ($m_i \approx 40$) as in Q-machines, the required field becomes almost prohibitively large (even though T_e is low $\approx 0.1 - 0.2$ eV). It was for this reason that a careful alignment of the wire exciter was essential for the pure IBW excitation experiment in the Q-machine.[6] Generally, it was advantageous to use low-mass ion plasmas such as hydrogen and helium for the investigation of cold-electron ion cyclotron waves. Fortunately, both the L-4 and ACT-1 devices had a relatively high (steady-state) magnetic field of 4 - 5 kG. For the investigation of hot electron modes, the requirement is much less stringent. It is however important to keep the parallel wave phase velocity near the valley of ion and electron Landau damping, $V_{Ti} << \omega / k_{\parallel} << V_{Te}$. In this case, it was often advantageous to go to heavier ion plasmas such as neon or argon since it is easier to establish the low Landau damping condition.

B. Ion concentration measurements for the multi-ion species plasmas.

A plasma can naturally contain more than one ion species, e.g. the impurity ions. It is also well known that a hydrogen discharge plasma usually contains three types of ions, H_1^+, H_2^+, and H_3^+. For the investigation of ion cyclotron waves, it is important to determine the concentration of respective ion species, particularly when examining multi-ion-species phenomena such as the ion-ion hybrid resonance. In L-4, using a neon-helium plasma, a spectroscopic method was used to measure the ion concentrations.[11] Figure 5 shows the measured wavelength of an ES ICW in a helium-neon mixture plasma, plotted as a function of the measured concentration. A strong ion concentration dependence is seen. The solid curve, which presents the calculated value from the wave dispersion relation, shows a good agreement with experiment.

It was later discovered that the cold electrostatic ion cyclotron wave (CES ICW) is particularly well suited for the ion concentration measurements [see Eq. (9)].[12] In ACT-1, in addition to the CES ICW method, the ion concentration of hydrogen was also deduced by analyzing the different branches of the IBW dispersion relation.[22]

C. Warm ion plasmas in ACT-1

In order to investigate finite ion temperature effects, one clearly needs a plasma with a finite ion temperature. But due to the presence of the neutral particles, the ion temperature of the weakly ionized filament discharge plasma in L-4 was quite low, $T_i <$ 0.1 eV. In such plasmas, the ionization fraction is relatively small – often well below 1 %. The neutrals, continuously in contact with the vacuum vessel wall (at room temperature), are quite effective in cooling the ions. The electron temperature on the other hand is relatively high, in the range of few eV. Electrons remain hot since the electron-ion collisional energy transfer rate is much lower than the corresponding ion-ion or ion-neutral rates. Indeed, low ion temperature behavior was observed in the dispersion relation of the electrostatic ion cyclotron waves in the L-4 device. As shown in Fig. 6, the measured dispersion relation agrees well with an ion temperature of 1/40 eV, i.e., room temperature.[10,11] But even at this low ion temperature, it is interesting to note that the ES ICW dispersion relation shows a clear FLR gap near $\omega \approx 2\Omega_i$.

The new type of plasma obtained in the ACT-1 toroidal device proved well suited to the full exploration of FLR waves. As described above, the combination of high ionization and low neutral-cooling rates yielded warm ions in the ACT-1 plasmas with ion temperatures approaching the electron temperature (a few eV). Indeed, it was found that the ion temperatures scaled roughly inversely with the neutral fill pressures.[21,22,24] In Fig. 7, the measured ion temperatures for plasmas with various

ion species are plotted versus the absolute neutral pressure. Doppler measurements of ion lines as well as the FLR dispersion relations of the ES ICW and IBW were used for the ion temperature measurements. As shown in the figure, by adjusting the neutral fill pressure, it was possible to vary the ion temperature over almost two orders of magnitude in the experiment, providing a method of control that was highly useful in the investigation of FLR effects.

INVESTIGATION OF WAVE DISPERSION RELATIONS

In this section, we summarize the investigation of electrostatic waves in the ion cyclotron range of frequencies in L-4 and ACT-1. Due to the space limitation, we only highlight the results which can be considered the experimental "first" and refer the readers to the original papers and theses manuscripts for more detail.

A. Electrostatic Ion Cyclotron Waves

Electrostatic ion cyclotron waves (ES ICW) in a two-ion-species plasma were investigated in the L-4 device.[9-11] The experiments confirmed that in a two-ion-species plasma, the relative motion of the ions of the two species is able to drive a new type of parametric instability.[10] The process had been predicted by theory.[8] A byproduct of this investigation was the verification of the ES ICW dispersion relation in a two-ion-species plasma. In particular, as seen in Fig. 6, the ion-ion hybrid resonance together with the FLR modification of the dispersion relation near the second harmonic frequency were both observed, even though $T_i \approx 1/40$ eV.

B. Cold Electrostatic Ion Cyclotron Waves

Utilizing the unique capability of the L-4 device (long device length, high field, and relatively cold electrons), the CES ICW could be excited by a slow-wave antenna in a helium-neon plasma. The experimental set-up is shown in Fig 8 (a). The slow-wave antenna consisted of four alternately phased elements comprising two axial wavelengths with $\lambda_{\parallel} = 62$ cm. As noted above, this cold mode can be launched quite easily from an external antenna (provided that it satisfies the cold electron condition) through the EPW $\rightarrow$ CES ICW mode-transformation process (at $\omega \approx \omega_{pi}$). The propagation characteristics, the wavelengths, and the damping were measured by a set of radial probes. Figure 8(b) displays a typical radial interferogram. From such data, the radial wavelength can be seen to decrease rapidly as the wave frequency approaches the ion-ion hybrid frequency, $\omega \rightarrow \omega_{ih} \approx 0.68\ \Omega_{He}$, confirming resonance behavior. The measured dispersion relation is shown in Fig. 8(c) for two concentrations (as marked). The solid curves present theoretically computed values that include finite electron

temperature effects. The agreement between theory and experiment is excellent. Backward propagation and resonance cone behavior were both confirmed. Also, near the ion-ion hybrid frequency, enhanced wave damping was measured. This same mode was later utilized in ACT-1 for measuring the hydrogen ion concentration, since the propagation angle depends only on the ion concentration (for a given value of magnetic field and wave frequency).[21]

C. Ion Bernstein Wave ($\omega / k_{\parallel} > V_{Te}$)

The ACT-1 toroidal device was used for a detailed experimental determination of the IBW dispersion relation, Eq.(1). In Fig. 9(a), the measured wave interferogram is shown as a function of the normalized frequency, ω/Ω_H. The wave exhibits a cut-off behavior ($\lambda \rightarrow \infty$) for $\omega \rightarrow 2\Omega_H$. In Fig. 9(b), the wave interferometer output is shown as a function of phase shift. The wave phase front moves toward the antenna while the wave packet is moving away from the antenna, confirming the backward-propagating character of the IBW. The experimental dispersion relation is plotted in Fig. 9(c). The solid curves show the theoretical values, Eq. (1), for various ion temperatures. Best agreement is seen for $T_i = 1.5$ eV. Such measurements can therefore be used to assess the hydrogen bulk-ion temperature for a plasma.[22] In Fig. 10, a more complete IBW dispersion relation measurement is shown. The CO_2-scattering data points, shown by the circles, agree well with the probe data (solid triangles).[22,24] The multiple branches of the dispersion relation reflect the presence of deuterium-like and tritium-like hydrogen molecular ions, H_2^+, and H_3^+. Corresponding theoretical dispersion curves are also shown.

D. Neutralized Ion Bernstein Wave ($\omega / k_{\parallel} < V_{Te}$)

The neutralized ion Bernstein wave (NIBW) or the backward branch of the electrostatic ion cyclotron wave was also observed in the ACT-1 neon plasma. This branch was predicted in the 60's when FLR effects were included in ES ICW dispersion relation.[1] Verification of this hot-ion branch was made possible by the creation of a low-collision finite-ion-temperature neon plasma in ACT-1.[27,28] In the experiment, a phased antenna structure immersed in the plasma was used to launch waves with a parallel phase velocity that satisfies the condition for propagation ($V_{Ti} << \omega / k_{\parallel} << V_{Te}$). In Fig. 11, the measured dispersion relation is shown by the open triangles and dots, and the theoretical solution of the dispersion relation is shown as a solid curve. The part of the dispersion curve that has a negative slope is the backward branch, and the place where the curve turns downward is the mode-conversion point. Experimental data are seen to yield quite good agreement with the theoretical curve.

MODE-TRANSFORMATION AND MODE-CONVERSION PROCESSES

A. Mode-transformation of EPW into IBW (ω = a few Ω_i)

As mentioned above, the EPW → IBW mode-transformation process can be used to launch the IBW from an external antenna. Since the IBW is a mode that only exists in a finite ion-temperature plasma, it is important to understand the EPW region that connects the IBW region with the external antenna. The excitation of the EPW by an external antenna has been investigated in detail for the lower hybrid wave heating,[36,37] and this mode-transformation process has been observed and studied in detail in ACT-1 warm hydrogen plasmas.[20,21] By changing the neutral pressure in ACT-1, the ion temperature could be varied over a wide range (1/40 eV to 2 eV), and Fig. 12(a) shows the interferogram output for several neutral pressures, as labeled. For the high-pressure case, the ions are essentially cold. The excited wave is an EPW that stays near the plasma edge, on the low density side of the cold plasma resonance or the lower hybrid resonance [shown for the $T_i \approx 0$ case in Fig. 12(b)]. As the neutral pressure is reduced (T_i increased), a gradual transformation into an IBW is observed. In Fig.12(b), the measured wave number (dots) is plotted as a function of radial position in the low-pressure warm-ion plasma. The solid curve is derived from Eq. (1) for T_i = 1.5 eV; the dashed curve is for $T_i = 0$. As expected, no sign of discontinuity was observed near the transformation region, the cold plasma resonance, in the experiment as long as T_i was held sufficiently high ($T_i \geq 0.5$ eV).

The transition from EPW ($\omega > \omega_{pi}$) to IBW ($\omega < \omega_{pi}$) can also be seen clearly in Fig. 13 (a), where the wave-packet amplitude (heavier curve) and interferogram output (lighter curve) are shown for various central plasma densities (labeled). The higher central density implies a larger density gradient. In the figure, the radial position of the cold lower-hybrid resonance layer which separates the EPW and IBW regimes is indicated by a dashed curve, and one sees that the wave transition between the two regimes is quite smooth. It is particularly interesting to note here that the IBW was launched effectively even when the ω_{pi} layer almost reached the limiter radius, approaching within a few millimeters of the antenna surface. Figure 13(b) shows the calculated ray position for various $\lambda_{||}$ (as labeled), with corresponding plasma parameters. The position of the wavepacket follows that of a ray for $\lambda_{||} \cong 36$ cm, which is the dominant launched $\lambda_{||}$ in the experiment. The IBW wavepacket is seen to display a dispersive characteristic (spreading of its trajectory due to the spread in $\lambda_{||}$) while the EPW wavepacket shows a resonance-cone characteristic.

A similar launching at the third ion-cyclotron harmonic was also demonstrated in ACT-1. In Fig. 14(a), the measured wave dispersion relation of the excited IBW is

shown by the dots. The calculated values are shown by the solid curves for various values of ion temperature. In Fig. 14(b), the measured wavenumber is plotted as a function of the plasma position (dots). As in Fig. 14(b), the theoretical values for T_i = 2 eV and T_i = 0 eV are shown. Again, a smooth mode-transformation could be seen across the cold LH resonance layer in a good agreement with theory. In this third harmonic launching case, a higher ion temperature (T_i = 2 eV) was required for efficient IBW launching as expected.

One should note that the external launching of the cold electrostatic ion cyclotron wave (CES ICW) also involves mode transformation of the launched EPW into a CES ICW near the ion plasma frequency. In this case, FLR effects are not important (except when the CES ICW approaches the ω_{ih} resonance). This manner of external CES ICW launching was demonstrated in the L-4 experiment described above.

B. Mode-conversion in the lower hybrid waves ($\omega >> \Omega_i$)

As the lower hybrid wave or EPW approaches the lower hybrid resonance, the FLR term becomes larger and the mode conversion into hot plasma waves (HPW) takes place. This process, predicted by Stix, can provide a mechanism through which ions are heated near the conversion layer.[3] Previous attempts to detect the mode-conversion process in several experiments were not successful partly due to the relatively cold-ion collisional plasmas. The ACT-1 plasma provided an ideal test bed to explore this long outstanding physics problem. The process nevertheless is complex in that the mode-conversion point for the each $k_{||}$ component is different both radially and toroidally, resulting in a complex interference pattern. In ACT-1, a significant broadening of the resonance cone was observed near the lower-hybrid resonance layer, Fig. 15.[26] The observed interference pattern revealed a periodic structure near the ion cyclotron harmonic frequencies, marking the influence of FLR effects. Modeling the experiment with a hot-ion electrostatic ray tracing code together with the Fourier reconstruction of the waveforms offered additional confirmation that linear mode conversion into HPW indeed occurred in the experiment.

VI. Application of IBW for plasma heating

In ion Bernstein wave heating (IBWH), a FLR wave, rather than the usual cold plasma wave, is used to transport the rf power to heat the plasma core in a tokamak reactor.[14,25] Careful investigation of the IBW has brought to light unique properties of the wave that are attractive for reactor application. Early wave accessibility studies showed that this FLR mode would be able to penetrate to the hot dense reactor plasma core without significant attenuation. Further investigation revealed additional useful

properties. Due to the low phase velocity ($\omega / k_\perp = V_{Ti} << V_\alpha$, where V_α is the velocity of the fusion alpha particles), wave absorption by the 3.5 MeV fusion α-particles, a potentially serious problem, can be avoided. Also, the FLR wave property that $k_\perp \rho_i \approx 1$ makes localized bulk ion heating possible at the ion cyclotron harmonic layers. Such heating of the bulk ion distribution can be desirable for optimizing fusion reactivity. Finally, the EPW-IBW mode transformation permits utilization of a lower-hybrid like waveguide launcher that is compatible for reactor application, as shown in Fig. 16.

The first IBW heating experiment was conducted in the ACT-1 toroidal device.[23] Using probe diagnostics, the physics of IBWH were investigated for all phases of the wave-heating scenario: IBW launching, propagation, absorption and heating.[20,-23] In a hydrogen plasma ($T_e \approx 2.5$ eV, $T_i \approx 1.5$ eV, and $n_0 \leq 10^{11}$ cm^{-3}), detailed profile measurements of the wave absorption and the resulting ion-temperature increase identified the heating layers near the ion cyclotron harmonics of deuterium-like (H_2^+) and tritium-like ions (H_2^+), where the dominant absorption resonances exist at $5\Omega_D$ and $5\Omega_T$.[23] Figures 17 and 18(a) show T_i versus frequency and radial position, confirming that the maximum ion temperature increase indeed occurred near the heating layer. In this experiment, the antenna phase was chosen to avoid electron Landau damping of the wave. Interestingly, as shown in Fig. 18 (b), the central ion heating efficiency actually increases with rf power, as higher T_i improves wave penetration. In the lower temperature range, collisions caused partial absorption of IBW power near the plasma edge. As the ions are heated, the higher T_i increases the group velocity (since $V_g \propto V_{Ti}$) and reduces the collisional absorption (Im $k_\perp \propto V_{Ti}^{-4}$). In the best case, power balance estimates suggest that the ion heating is nearly 100% efficient for IBWH. Moreover, ion energy analyzer data showed that the heat deposition was into the bulk ions without any significant production of an ion tail. This characteristic of IBWH can be explained by quasilinear-diffusion / Fokker-Planck collision theory[42] in the large FLR limit.[25]

The B_θ-loop was also tested on ACT-1, where the physics of IBWH wave loop-excitation and the antenna loading was investigated in considerable detail.[29,31] After the ACT-1 experiment, IBW heating was investigated in many tokamak devices including JIPPTII-U, TNT, PLT and Alcator-C, JFT-II-M, DIII-D, and PBX-M. The first waveguide IBW experiment is planned on the FT-U tokamak. A review article summarizing the IBW-related activities can be found in Ref. 25.

PARASITIC EXCITATION OF ELECTROSTATIC WAVES

Electrostatic waves can be excited inadvertently in high-power ICRF experiments. The anomalous antenna loading observed during the Faraday-shield-less operation of the Ion Cyclotron Wave Heating (termed Mode X) may be one well known example.[39] Mode X may be the actual external launching of a CES ICW which unfortunately cannot propagate to the plasma core. It was noted earlier that in L-4, various parametric excitations of electrostatic waves during the ICRF were investigated.[9-11] And in ACT-1, two dominant parasitic IBW excitation processes by the near field of the Faraday-shielded ICRF antenna have been observed.[29,30]

Parametric Instabilities - With relatively low threshold electric field, strong parametric instability activity has been observed where the ion Bernstein wave and an ion quasi-mode are excited as the lower sideband and low-frequency mode, respectively.[30] Figure 19 portrays the observed instability amplitude and the calculated growth rate. Agreement between the observed amplitude and the calculated growth rate is quite good, especially considering that the observed amplitude is the nonlinear saturated value of the unstable mode. Due to a quite restrictive selection-rule condition, parametric IBW excitation is not likely to play an important role under normal fast-wave heating conditions. The likelihood of excitation will, however, increase for higher frequency operation ($\omega >> 2\Omega_i$) due to a lower power threshold and to the availability of more decay modes.

Density Gradient Excitation - Ion Bernstein waves can also be excited through a density-gradient-driven process.[29] In Fig. 20, a two-dimensional wave interferogram of the excited IBW is shown. Noting that the excitation efficiency depends on the density gradient in front of the antenna, one may attribute the nonuniform excitation pattern to the nonuniform density gradient along the antenna surface. In the context of the slab model, the E_y field of the fast-wave antenna couples to the IBW E_x field through the spatial derivative term, $\partial_x K_{xy}$ in the density gradient region. A theory based on a local analysis of the Vlasov-Maxwell equations including the effect of the plasma density gradient was developed and found to be in very good agreement with the experimental observation.[29] Such a process can assume increased importance if the antenna loading into the fast wave is not sufficiently high, a condition that may occur if the antenna-plasma gap distance is increased.

CONCLUDING REMARKS

In conclusion, a variety of electrostatic waves and related processes in the ion cyclotron range of frequencies were investigated in L-4 and ACT-1. Almost every successful experimental measurement showed surprisingly good agreement with the FLR magnetized wave theory developed by Stix,[1] Bernstein,[33] and others. However, this fact certainly did not diminish the satisfaction of actually observing the predicted phenomena for the first time. One is usually unsure until the phenomena are actually observed in an experiment. After confirmation, they can be treated as something obvious. This sequence is, in fact, the important function of experiments. Once waves were well understood in both theory and experiment, they often served as useful tools for plasma diagnostics, e.g., EPW for n_e, ES ICW for T_e, T_i, and n_i, IBW for T_i, and n_i, etc. However, it was not always easy to predict the outcome of an experiment. In dealing with actual experimental situations there are many possible reasons for not observing the expected phenomena. Excessive fluctuations, for example, can mask the phenomena being investigated. Some waves are more susceptible to fluctuations than others. The neutralized IBW was a relatively difficult wave to detect and the reason for the difficulty is not fully understood even today. The search for the mode-converted hot-plasma waves near the lower-hybrid resonance was also quite complicated and required a sophisticated analysis. On the other hand, some experiments turned out to be easier than expected. Experiments to externally excite the CES ICW and IBW are examples. In ACT-1, the IBW was observed almost immediately after the "switch" was turned on. We were especially impressed by the coherence of IBW propagation in ACT-1. And indeed, the effect of fluctuations on IBW was later calculated to be relatively small.[43] Through experimental investigation, we came to appreciate wave absorption processes such as ion cyclotron damping and electron Landau damping. We also became keenly aware of nonlinear processes even when investigating processes that were nominally linear.

Looking to the future, I believe that such basic physics experiments are enormously useful for the main-line fusion program. They are certainly important for the current IBW experiments in large tokamaks. IBW heating, moreover, appears to have many applications in addition to heating fusion plasmas (see Ref. 25 for example). Areas of application for these waves may include astronomical as well as industrial plasmas.

I would like to conclude this paper by adding one more possible application for these waves. For a fusion reactor, impurity control and removal of helium ash are important issues. The ash accumulation, if unchecked, can degrade or even quench the fusion reaction. The helium ash is a noble gas and rather difficult to pump compared to

other more reactive gases. There are several ideas for pumping helium ash by selective heating near the plasma edge. As the helium ions are heated in the edge region, they can be trapped by the field ripple (natural or created) which then can cause the trapped helium ions to drift rapidly out of the plasma. A trap of some sort could, presumably, then capture them. This scheme would pump helium both as it comes out from and as it re-enters the plasma. In principle, the scheme can be used for other impurity ions as well. The idea is certainly not new – fast-wave heating has already been suggested for this purpose.[44] However, the selective local absorption of the fast wave by the minority helium ions in the low temperature, low-β edge region may not be efficient. One possible improvement proposed here is to use the externally launched ion Bernstein wave (IBW) or the cold electrostatic ion cyclotron wave (CES ICW). Both electrostatic waves can be used to heat the helium resonance with relatively high efficiency even at the edge. Although not suited for core plasma heating, the CES ICW should work well for such edge heating. External launching of both waves was already demonstrated in the L-4 and ACT-1 experiments. Singly ionized helium ions have a unique ion cyclotron layer and, therefore, may be selectively heated. Moreover, the wave fields of those externally launched electrostatic waves can be localized toroidally. For IBW, one might heat at $3\Omega(^4He)$ using $2\Omega_D$ launching or at $5\Omega(^4He)$ using $4\Omega_T$ launching. For the CES ICW, an obvious choice is $\Omega(^4He)$ heating using Ω_T launching. It should be noted here that the FLR modification of the CES ICW in the region between the tritium-helium ion-ion hybrid frequency and the helium ion-cyclotron frequency would be expected to improve the power absorption. Even though the required ion energy for helium removal is not known precisely (but probably in the range of few hundred to few keV), the longer wavelength of the CES ICW could well result in heating the helium ions to higher energy compared to IBW. This manner of ash removal can be investigated in the present-day tokamaks using existing IBW antennas (such as in PBX-M), since the IBW-type antenna is well suited to launch both the IBW and the CES ICW.

Acknowledgments: The author is deeply indebted to Dr. Stix' teaching of waves through his class, his books and manuscripts, and frequent private discussions. He also thanks him for giving much needed guidance, support, and encouragement over years for the work described here. The author would like as well to express his appreciation to his former Ph. D. advisors, Drs. M. Porkolab and R. P. H. Chang. He also thanks Dr. K. L. Wong for his contributions to the work presented here through the ACT-1 device construction and subsequent experiments. This work also describes the doctoral thesis work performed by the former ACT-1 students, Drs. G. A.Wurden, F. N. Skiff, and J. A. Goree. This work was supported by U.S. Department of Energy contract No. DE-AC02-76-CHO-3073.

REFERENCES

1. T. H. Stix, Theory of Plasma Waves (McGraw-Hill, New York 1962). See also Waves in Plasmas (AIP, New York 1992).
2 D. G. Swanson and Y.C. Nygan, Phys. Rev. Lett. 35, 517 (1975).
3. T. H. Stix, Phys. Rev. Lett. 15, 878 (1965).
4. A. Y. Wong, N. D'Angelo, and R. W. Motley, Phys. Rev. Lett. 9, 415 (1962).
5. E. R. Ault and H. Ikezi, Phys. Fluids 13, 2874 (1970).
6. J. P. M. Schmitt, Phys. Rev. Lett. 31, 982 (1973).
7. S. J. Buchsbaum, Phys. Fluids, 3,418 (1960)
8. J. L. Sperling and F. W. Perkins, Phys. Fluids 17, 1857 (1974).
9. M. Ono, Ph.D. Thesis, Princeton University (1978).
10. M. Ono, M. Porkolab, and R.P.H. Chang, Phys. Rev. Lett.. 38, 962 (1977).
11. M. Ono, M. Porkolab, and R.P.H. Chang, Phys. Fluids 20, 1656 (1980), and 20, 1675(1980).
12. M. Ono, Phys. Rev. Lett. 42, 1267 (1979).
13. N. J. Fisch, Phys. Rev. Lett. 41, 873 (1978).
14. See National Technical Information Service Document No. PPPL-1593 ("Plasma heating by externally launched ion Bernstein waves," by M. Ono, 1979). Copies may be ordered from NTIS, Springfield, Virginia 22161; Phys. Fluids 28, 2645 (1985).
15. K. L. Wong, M. Ono, and G.A. Wurden, Rev. Sci. Instrum. 53(4), 409 (1982).
16. K. L. Wong, R. Horton, and M. Ono, Phys. Rev. Lett. 45, 117 (1980).
17. J. Goree, M. Ono, P. Colestock, R. Horton, D. McNeill, and H. Park, Phys. Rev. Lett. 55, 1669 (11985).
18. M. Ono, G. J. Greene, D. S. Darrow, C. Forest, H. Park, and T. H. Stix, Phys. Rev. Lett. 59, 2165 (1987).
19. C. B. Forest, Y. S. Hwang, M. Ono, and D. S. Darrow, Phys. Rev. Lett. 68, 3559
(1982).
20 M. Ono, K.L. Wong, Phys. Rev. Lett. 45, 1105 (1980).
21 M. Ono, K. L. Wong, and G. A. Wurden, Phys. Fluids 26, 298 (1983).
22 G. A. Wurden, M Ono, and K. L. Wong, Phys. Rev. A 26, 2297 (1982).
23 M. Ono, G. A. Wurden, and K. L. Wong, Phys. Rev. Lett. 52, 37 (1984).
24 G. A. Wurden, Ph.D. Thesis, Princeton University (1982).
25 M. Ono, Phys. Fluids B, Feb. (1993). A review article on IBW heating.
26. G. A. Wurden, K. L. Wong, F. Skiff, and M. Ono, Phys. Rev. Lett. 50, 1779 (1983).
27 J. A. Goree, Ph.D. Thesis, Princeton University (1985).
28 J. A. Goree, M. Ono, and K. L. Wong, Phys. Fluids 28, 2845 (1985).
29. F. N. Skiff, Princeton University, Ph.D. Thesis (1985).
30 F. N. Skiff, M. Ono, and K. L. Wong, Phys Fluids 27, 1051 (1984).
31. F. N. Skiff, M. Ono, P. Colestock, and K. L. Wong, Phys. Fluids 28, 2453
32. B. D. Fried and S. D. Conte, The Plasma Dispersion Function (Academic, New York, 1961).
33. I. B. Bernstein, Phys. Rev. 109, 10 (1958).

34. P. K. Fisher and R. W. Gould, Phys. Fluids 14, 857 (1971).
35. H. H. Kuel, Phys. Fluids 17, 1636 (1974).
36. P. M. Bellan and M. Porkolab, Phys. Fluids 17, 1592 (1974), and 19, 995 (1976).
37. S. Bernabei, M. A. Heald, W. H. Hooke, R. W. Motley. F. J. Paoloni,. M. Brambilla, and W. D. Getty, Nucl. Fusion 17, 929 (1977).
38. D. G. Swanson, Phys. Fluids 10, 1531 (1975).
39. M. A. Rothman, R. M. Sinclair, and S. Yosnikawa, J. Nuclear Energy, Part C, 8, 241 (1966).
40. D. G. Swanson, , Phys. Fluids 28, 2645 (1985).
41. R. Limpacher and K. R. Mackenzie, Rev. Sci. Instrument 44, 726 (1973).
42. T. H. Stix, Nucl. Fusion 15, 753 (1976).
43. M. Ono, Phys. Fluids 25, 990 (1982).
44. J. C. Hosea, Private Communication.

FIGURE CAPTIONS

Fig. 1. Behavior of wave dispersion relation near the lower hybrid resonance layer ($b = 0$). The solid curve shows a mode-transformation process for $\omega < 2\Omega_i$ ($a > 0$). The dashed curve shows a mode-conversion process typical for $\omega >> \Omega_i$ ($a < 0$).

Fig. 2. Schematic of experimental set-up in the L-4 linear device.

Fig. 3 Schematic of the ACT-1 device.

Fig. 4. Schematic of the tungsten filament plasma source in ACT-1.

Fig. 5. Ion concentration measurement in the L-4 helium-neon plasma. The dots are the measured ES ICW wavelength plotted as a function of the measured ion spectroscopic ion concentration ratio. The solid line shows theoretical values calculated from the wave dispersion relation.

Fig. 6. Electrostatic ion cyclotron waves in L-4. Dots are experimentally measured values. Solid and dashed curves are theoretical dispersion relations for various values of ion temperatures, as labeled. The ion-ion hybrid frequency is shown for $\omega_{ih} / \Omega_{He} = 0.51$. $B = 2.9$ kG and He:Ne = 4:6.

Fig. 7. Summary plot of ion temperatures as a function of absolute fill pressure for various operating gases in ACT-1 based on Doppler line broadening, electrostatic ion cyclotron wave, and ion Bernstein wave measurements.

Fig. 8. Investigation of cold electrostatic ion cyclotron waves in L-4. (a) Simplified schematic of wave propagation setup. (b) Radial interferometer output for various values of ω / Ω_{He} (as labeled) in He:Ne = 2:8 plasma. (c) Wave dispersion relation for two ion concentrations (as labeled). Dots are experimentally measured values and solid curves are theoretical values.

Fig. 9. Ion Bernstein wave identification in ACT-1. (a) Wave interferometer traces for various values of ω / Ω_H ($r = 2$ cm), as labeled. (b) Interferometer traces for various phase delays, $\omega \Delta t / 2\pi$. (c) Wave dispersion relation. Dots are experimental points and solid curves are the theoretical values.

Fig. 10. A complete IBW dispersion relation in ACT-1 hydrogen plasma. Solid triangles are probe values, open circles are the CO_2 laser points, and lines are

theoretical curves. Deuterium-like and tritium-like resonances are due to the H_2^+, and H_3^+ molecular ions.

Fig. 11. Dispersion relation for the electrostatic ion cyclotron wave in a neon plasma. Solid dots and open triangles display experimentally measured values while the solid curve is a numerical solution with $k_{||} = 1.0\ cm^{-1}$, $T_e = 2.1$ eV, and $T_i = 0.4$ eV. The negatively sloped part of the dispersion curve is the backward branch or the neutralized IBW.

Fig. 12. Verification of EPW-IBW mode transformation in ACT-1. (a) Interferometer traces for various neutral pressures. (b) Wave number versus radial position. Dots are experimental points and curves are theoretical values. $\omega / \Omega_H (r=0) = 1.9$. $p_H = 7 \times 10^{-6}$ Torr.

Fig. 13. EPW / IBW wave-packet radial profiles versus plasma density. (a) Radial wave packet amplitude profiles (thicker curves) and interferogram traces (finer curves) for various central densities (as labeled). (b) Corresponding wave-packet positions predicted from ray-tracing calculation for various $\lambda_{||}$. The dashed line ($b = 0$), $\omega = \omega_{pi}$, separates IBW and EPW regions.

Fig. 14. Third-harmonic launching of IBW in ACT-1. (a) $\omega \leq 3\ \Omega_H$ IBW dispersion relation. Dots are measured and solid curves are theoretical values for various T_i (as labeled). $r = 4$ cm, $B_0 = 4.3$ kG, and $n_e = 3\ 10^{10} cm^{-3}$. (b) Wavenumber vs. radial distance from the antenna. Dots are experimental points and curves are theoretical values. Lower hybrid resonance layer is indicated by a dashed line.

Fig. 15. Observation of lower-hybrid mode-converted hot-plasma modes in ACT-1. The radial wave amplitude is plotted as a function of applied rf frequency. Interference patterns caused by the incoming lower hybrid wave and the converted hot plasma mode can be seen in band above ion cyclotron harmonics.

Fig. 16 IBW heating configuration in typical tokamak parameters. (a) IBW waveguide launcher is shown on the left. Plasma cross-section is separated according to the various regimes. Going from low to high density, the electron plasma wave, ion Bernstein wave, and high β ion Bernstein wave regimes, respectively.

Fig. 17. Ion temperature versus frequency during IBW heating in ACT-1. (a) $\omega/\Omega_H = 1.6 - 1.9$. (b) $\omega/\Omega_H = 2.4 - 2.75$. $P_{rf} = 10$ W, $r = 3$ cm, $B_0 = 4.75$ kG, and $n_e = 2.5 \times 10^{10}\ cm^{-3}$.

Fig. 18. IBW heating experiment in ACT-1. (a) Ion temperature profiles for various rf power levels (as labeled). (b) Peak ion temperature versus rf power; f = 11.6 MHz, B_0 = 4.75 kG, $n_e = 2.5 \times 10^{10}\,cm^{-3}$.

Fig. 19. Parametric excitation of IBW in ACT-1. (a) Measured IBW decay wave amplitude versus ω(decay) / Ω_H. The toroidal field increases to the left. Ion cyclotron harmonic frequencies are indicated. (b) Calculated growth rate for the corresponding experimental parameters.

Fig. 20. Parasitic excitation of IBW in ACT-1. The measured ion Bernstein wave interferogram is plotted over the poloidal section of the plasma. In the toroidal direction, the probe is located 34 cm from the Faraday shielded ICRF antenna.

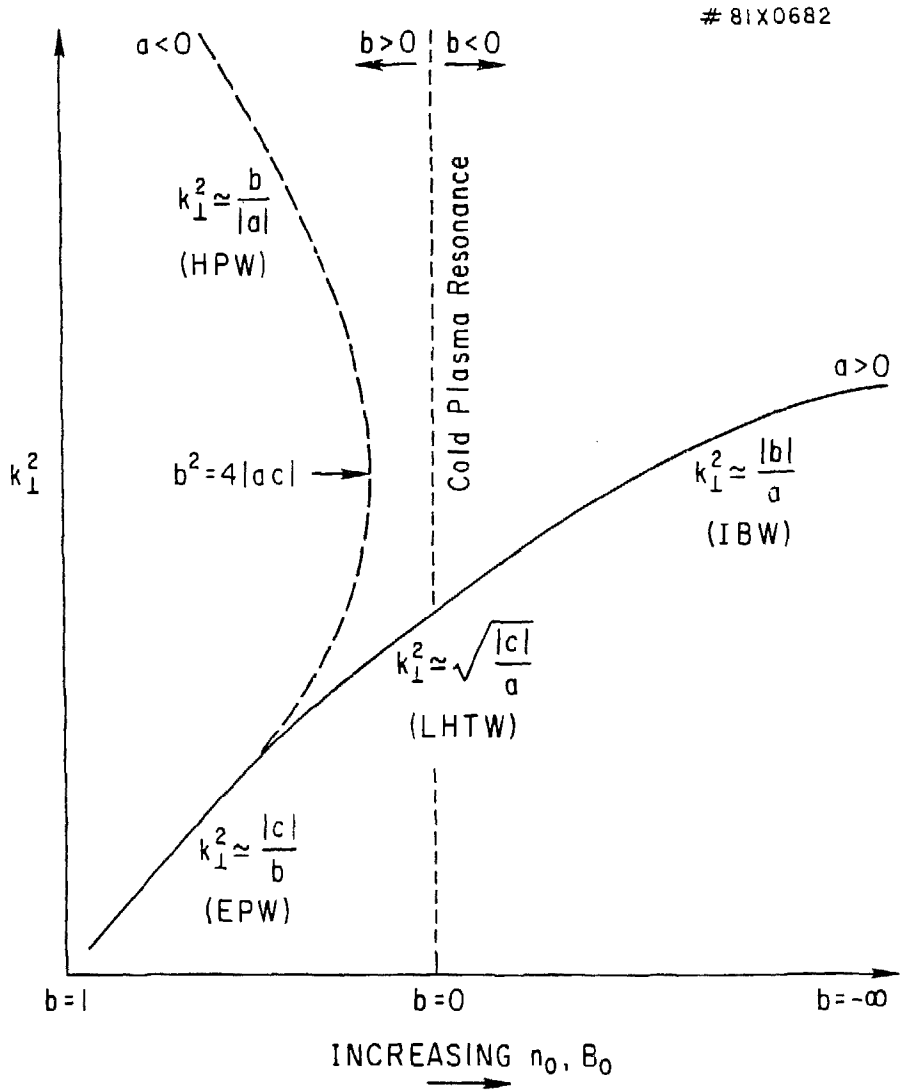
#81X0682
a<0
b>0
b<0
$k_\perp^2 \simeq \frac{b}{|a|}$
(HPW)
Cold Plasma Resonance
a>0
$k_\perp^2$
$b^2=4|ac|$
$k_\perp^2 \simeq \frac{|b|}{a}$
(IBW)
$k_\perp^2 \simeq \sqrt{\frac{|c|}{a}}$
(LHTW)
$k_\perp^2 \simeq \frac{|c|}{b}$
(EPW)
b=1
b=0
b=-∞
INCREASING n_0, B_0

Fig. 1

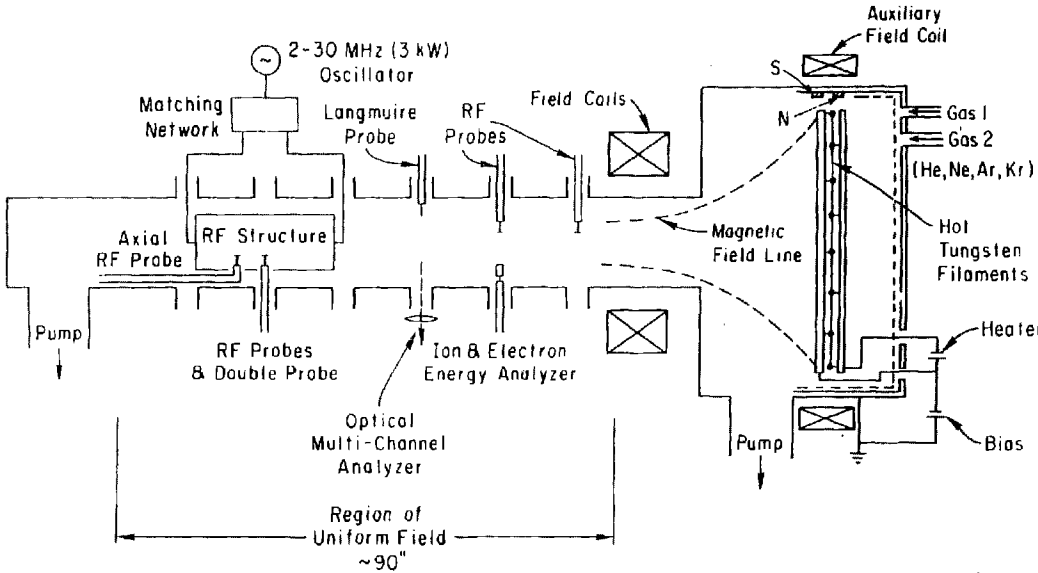
2-30 MHz (3 kW)
Oscillator
Matching
Network
Langmuire
Probe
RF
Probes
Field Coils
Auxiliary
Field Coil
S
N
Gas 1
Gas 2
(He, Ne, Ar, Kr)
Axial
RF Probe
RF Structure
Magnetic
Field Line
Hot
Tungsten
Filaments
Pump
RF Probes
& Double Probe
Ion & Electron
Energy Analyzer
Heater
Optical
Multi-Channel
Analyzer
Pump
Bias
Region of
Uniform Field
~90"

Fig. 2

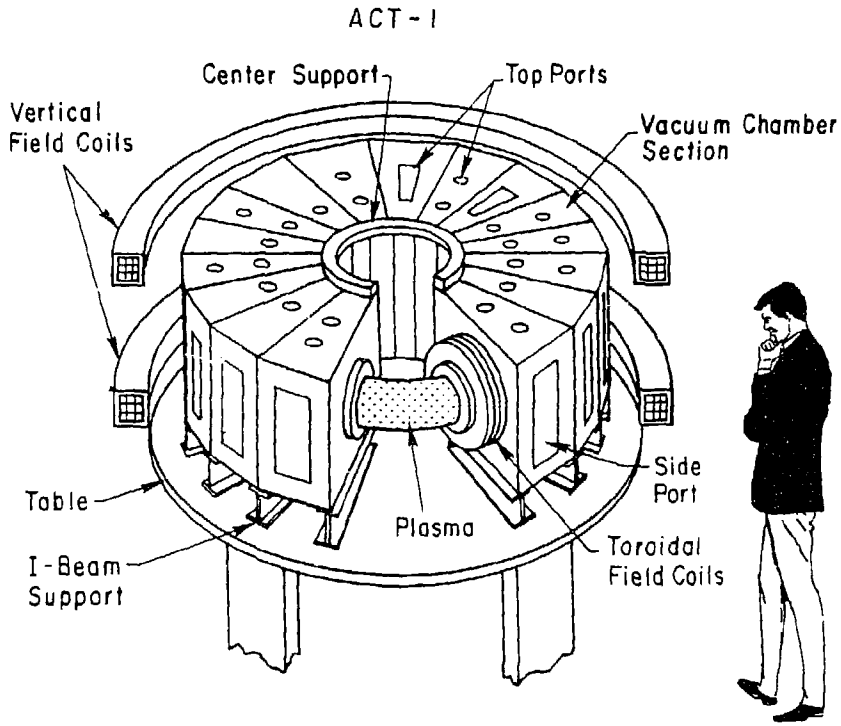
ACT-I
Center Support
Top Ports
Vertical
Field Coils
Vacuum Chamber
Section
Table
I-Beam
Support
Plasma
Side
Port
Toroidal
Field Coils

Fig. 3

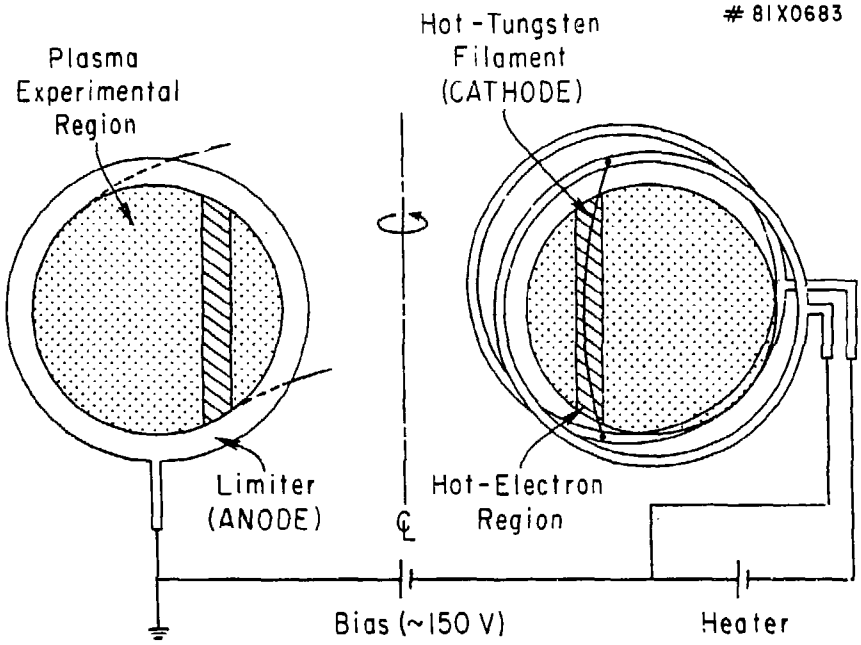
#81X0683
Hot-Tungsten
Filament
(CATHODE)
Plasma
Experimental
Region
Limiter
(ANODE)
Hot-Electron
Region
Bias (~150 V)
Heater

Fig. 4

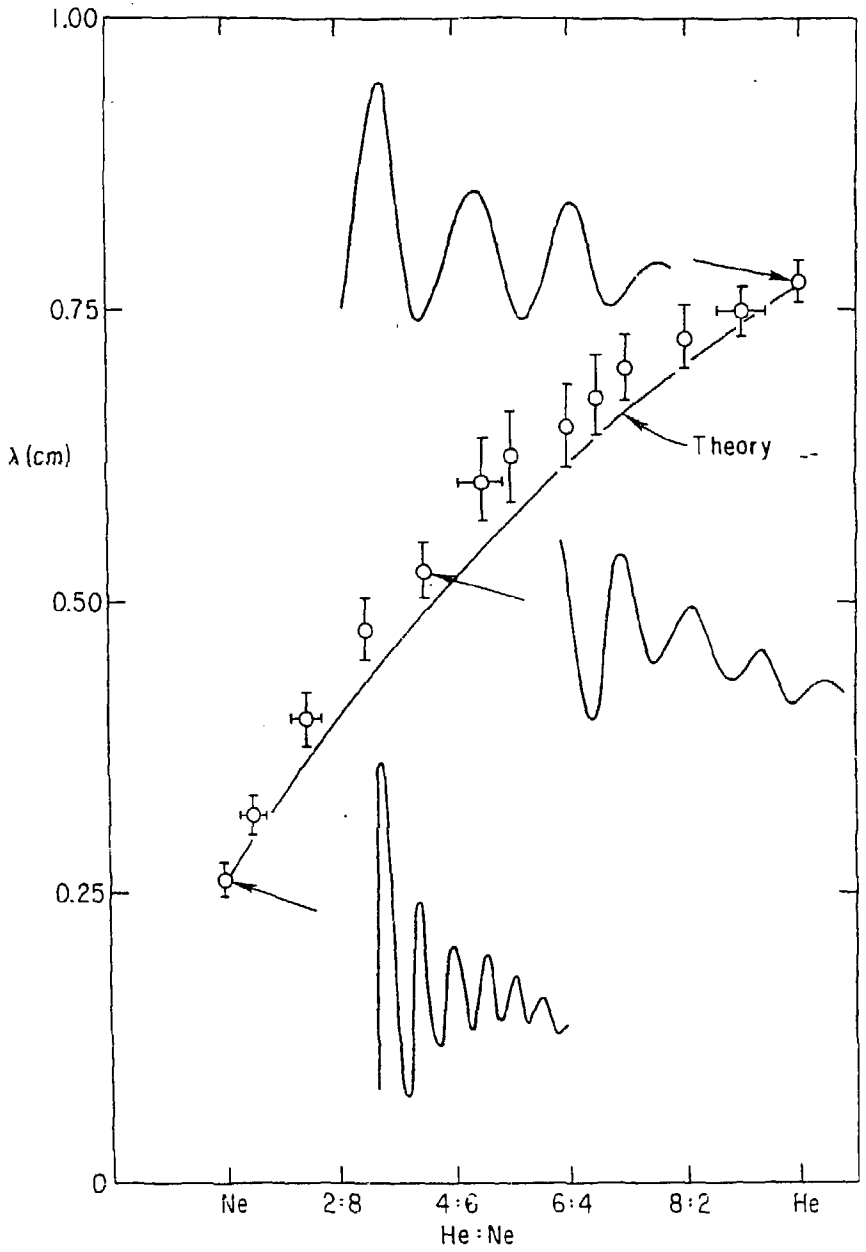

Fig. 5

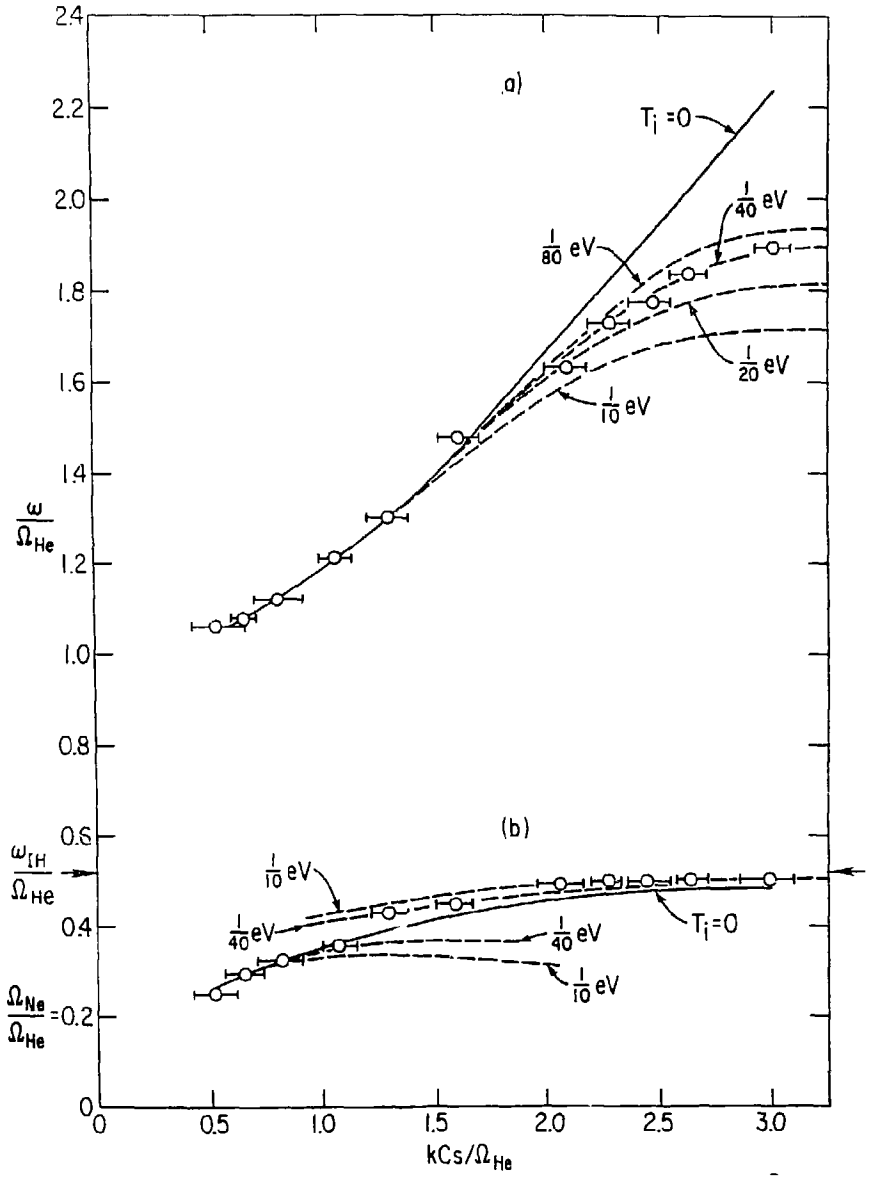
a)
$T_i = 0$
$\frac{1}{40}$ eV
$\frac{1}{80}$ eV
$\frac{1}{20}$ eV
$\frac{1}{10}$ eV
$\frac{\omega}{\Omega_{He}}$
(b)
$\frac{\omega_{IH}}{\Omega_{He}}$
$\frac{\Omega_{Ne}}{\Omega_{He}} = 0.2$
$T_i = 0$
kCs/Ω_{He}
0
0.5
1.0
1.5
2.0
2.5
3.0
0.2
0.4
0.6
0.8
1.0
1.2
1.4
1.6
1.8
2.0
2.2
2.4

Fig. 6

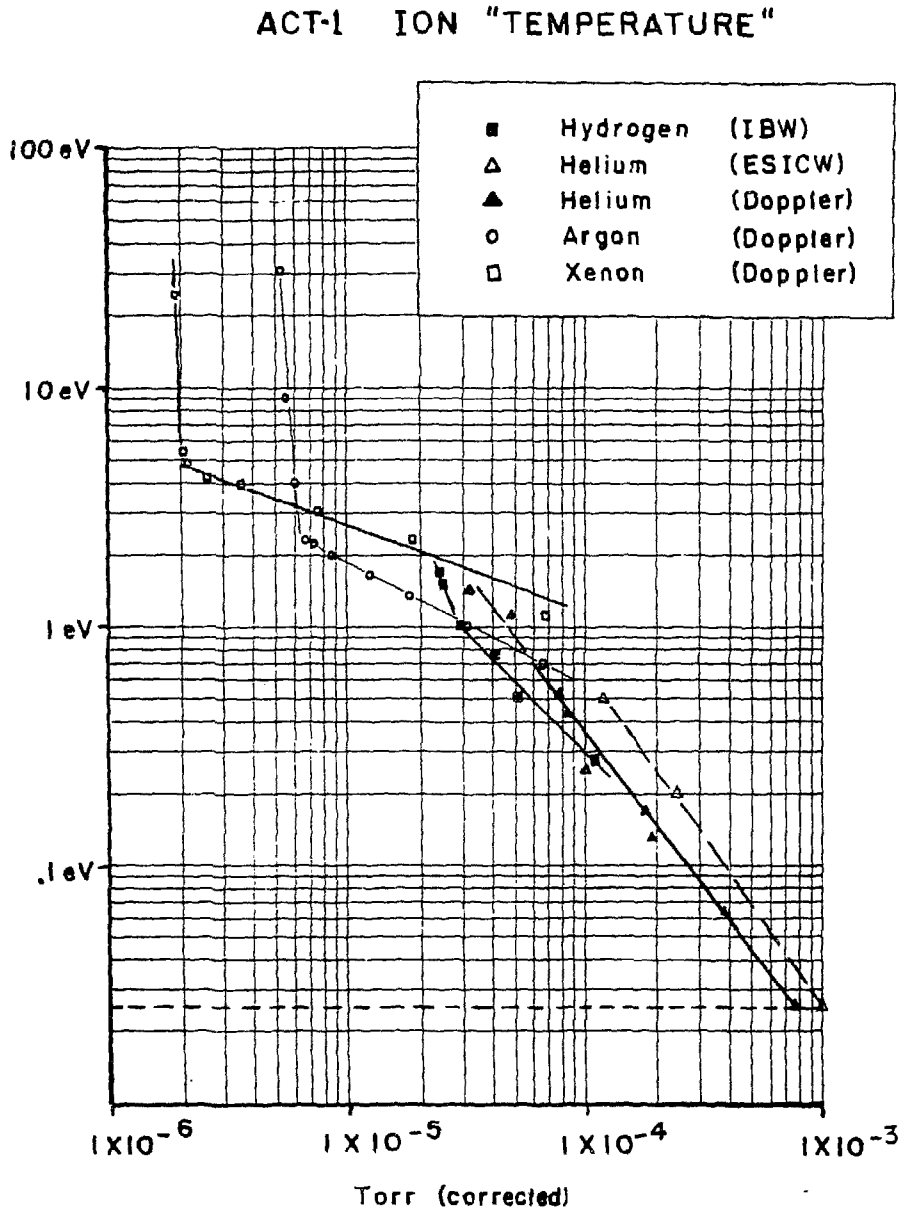
ACT-1 ION "TEMPERATURE"
Hydrogen (IBW)
Helium (ESICW)
Helium (Doppler)
Argon (Doppler)
Xenon (Doppler)
100 eV
10 eV
1 eV
.1 eV
1X10-6
1X10-5
1X10-4
1X10-3
Torr (corrected)

Fig. 7

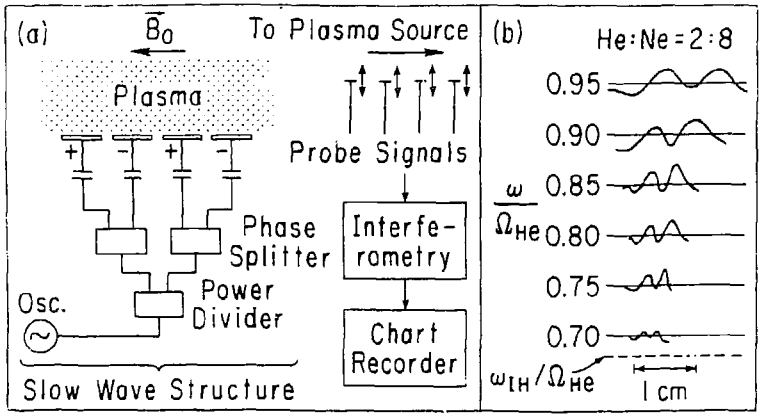
(a)
$\vec{B}_0$
To Plasma Source
Plasma
Probe Signals
Phase Splitter
Interfe-rometry
Power Divider
Osc.
Chart Recorder
Slow Wave Structure
(b)
He:Ne=2:8
0.95
0.90
0.85
0.80
0.75
0.70
$\frac{\omega}{\Omega_{He}}$
ω_{IH}/Ω_{He}
1 cm

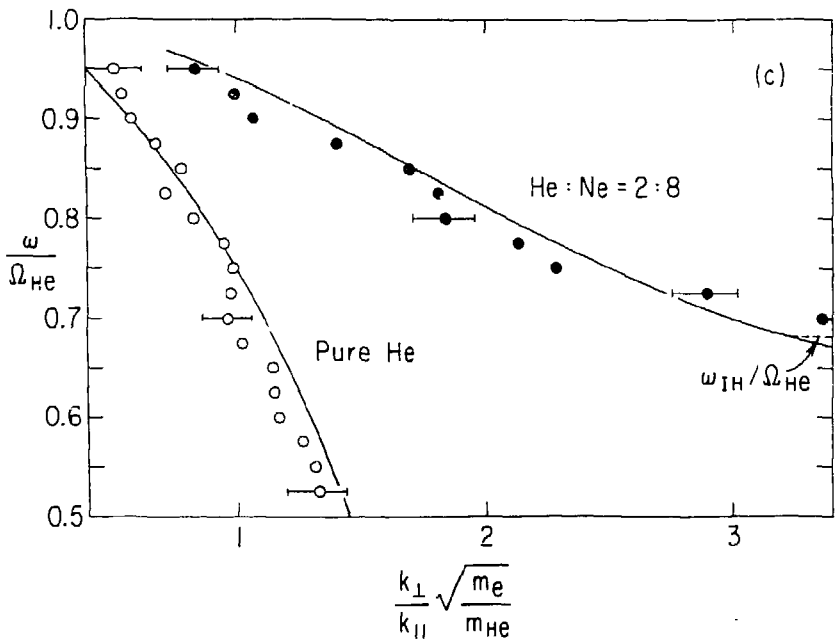
(c)
He : Ne = 2 : 8
Pure He
ω_{IH}/Ω_{He}
$\frac{\omega}{\Omega_{He}}$
1.0
0.9
0.8
0.7
0.6
0.5
1
2
3
$\frac{k_\perp}{k_{||}}\sqrt{\frac{m_e}{m_{He}}}$

Fig. 8

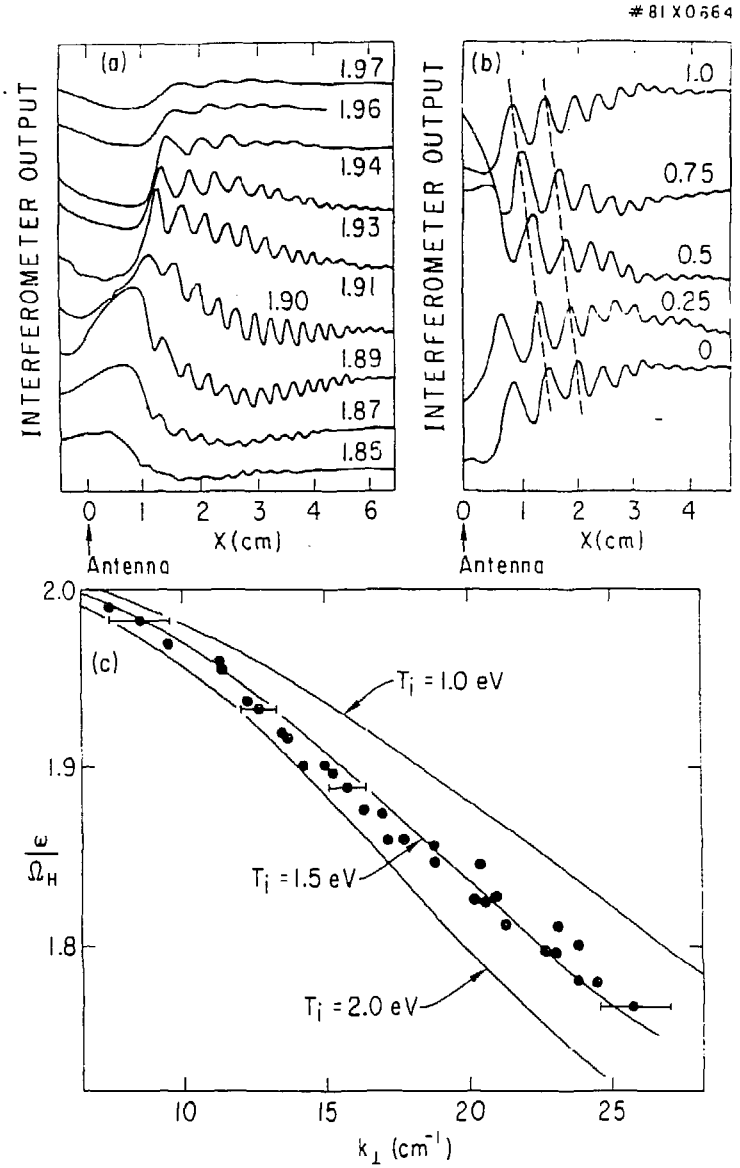
#81X0664
(a)
1.97
1.96
1.94
1.93
1.91
1.90
1.89
1.87
1.85
INTERFEROMETER OUTPUT
0 1 2 3 4 6
X(cm)
Antenna
(b)
1.0
0.75
0.5
0.25
0
INTERFEROMETER OUTPUT
0 1 2 3 4
X(cm)
Antenna
(c)
T_i = 1.0 eV
T_i = 1.5 eV
T_i = 2.0 eV
ω/Ω_H
2.0
1.9
1.8
10 15 20 25
$k_\perp$ (cm^{-1})

Fig. 9

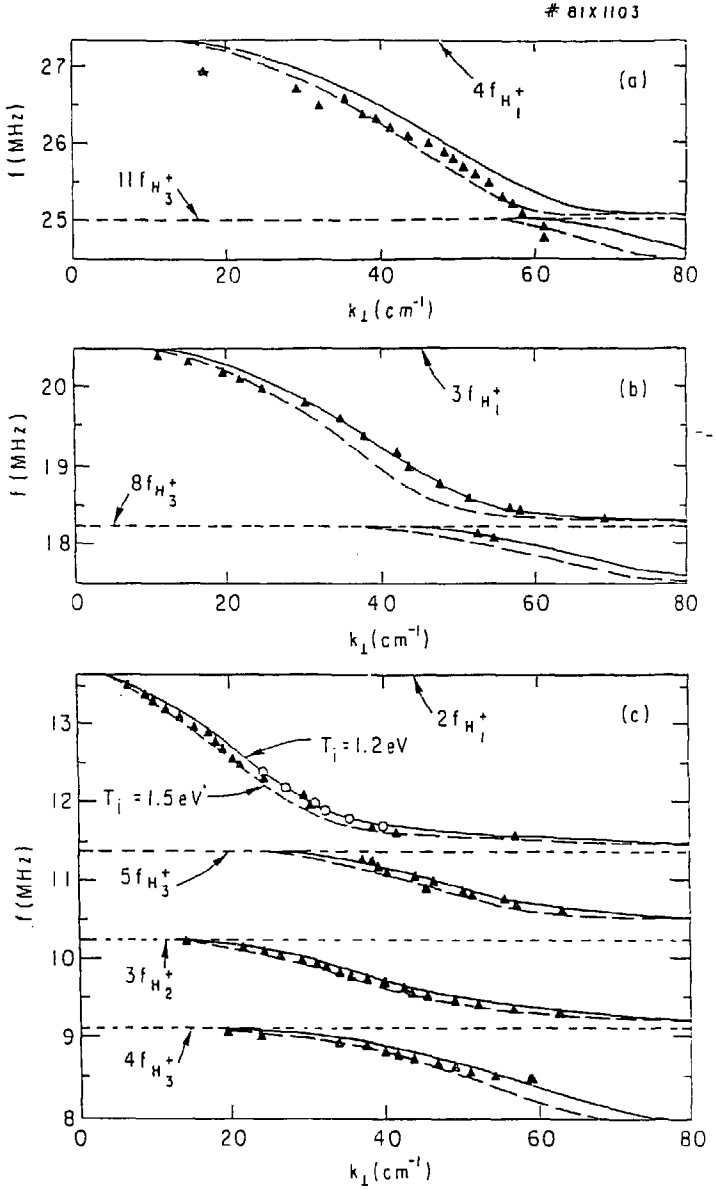
81X1103
(a)
$4f_{H_1^+}$
$11f_{H_3^+}$
f (MHz)
$k_\perp (cm^{-1})$
(b)
$3f_{H_1^+}$
$8f_{H_3^+}$
f (MHz)
$k_\perp (cm^{-1})$
(c)
$2f_{H_1^+}$
$T_i = 1.2 eV$
$T_i = 1.5 eV$
$5f_{H_3^+}$
$3f_{H_2^+}$
$4f_{H_3^+}$
f (MHz)
$k_\perp (cm^{-1})$

Fig. 10

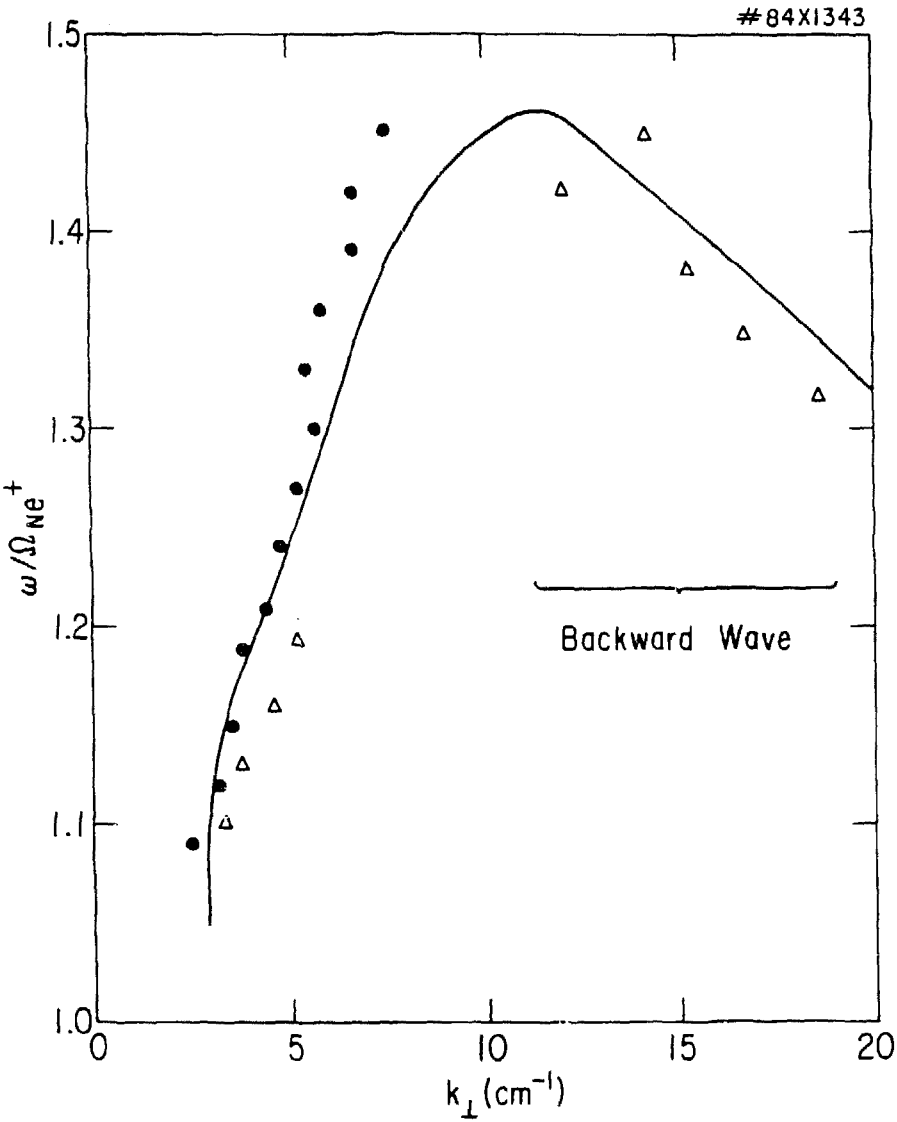
#84X1343
1.5
1.4
1.3
1.2
1.1
1.0
0
5
10
15
20
ω/Ω_{Ne^+}
$k_\perp (cm^{-1})$
Backward Wave

Fig. 11

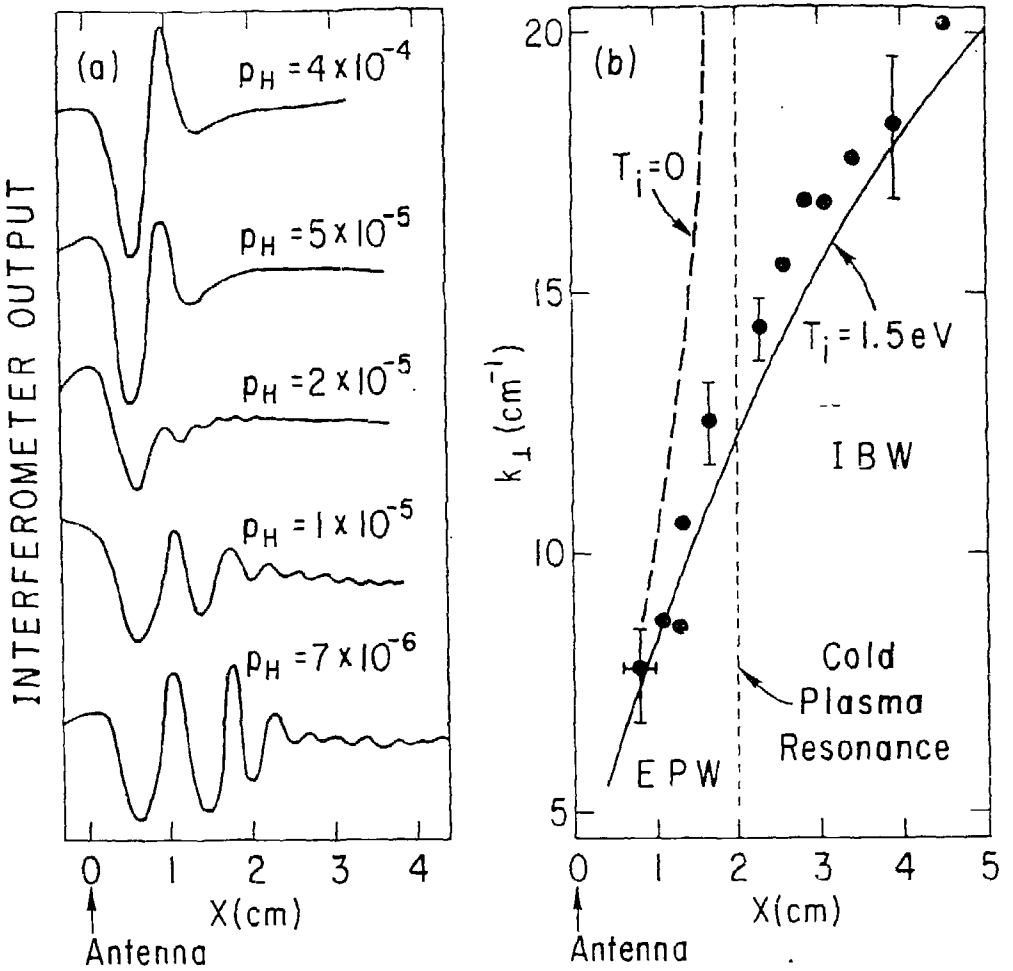
(a)
$p_H = 4 \times 10^{-4}$
$p_H = 5 \times 10^{-5}$
$p_H = 2 \times 10^{-5}$
$p_H = 1 \times 10^{-5}$
$p_H = 7 \times 10^{-6}$
INTERFEROMETER OUTPUT
0 1 2 3 4
X(cm)
Antenna
(b)
$T_i = 0$
$T_i = 1.5$ eV
IBW
Cold
Plasma
Resonance
EPW
$k_\perp$ (cm^{-1})
20
15
10
5
0 1 2 3 4 5
X(cm)
Antenna

Fig. 12

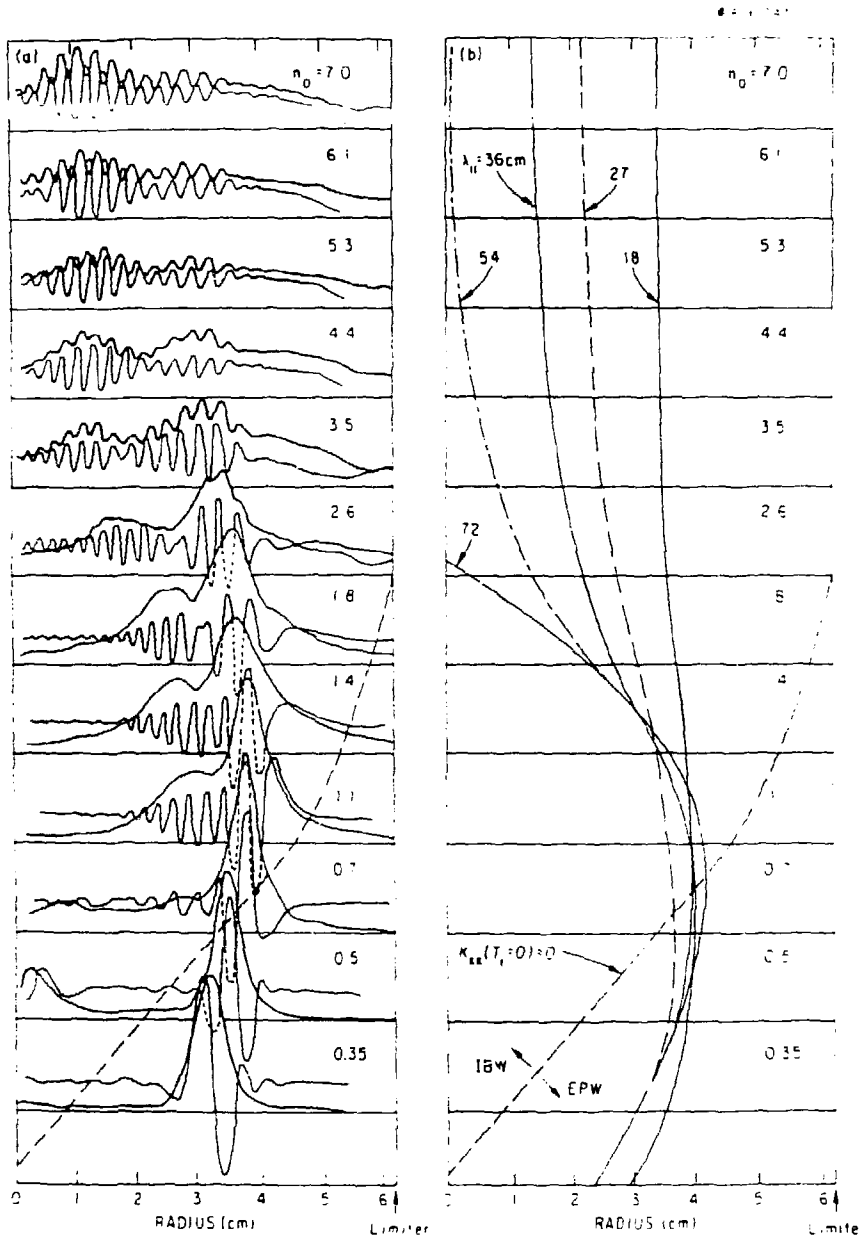
(a)
n_0=7.0
6.1
5.3
4.4
3.5
2.6
1.8
1.4
1.1
0.7
0.5
0.35
0
1
2
3
4
5
6
RADIUS (cm)
Limiter
(b)
n_0=7.0
$\lambda_{\parallel}$=36cm
27
54
18
72
$K_{ee}(T_e=0)=0$
IBW
EPW
RADIUS (cm)
Limiter

Fig. 13

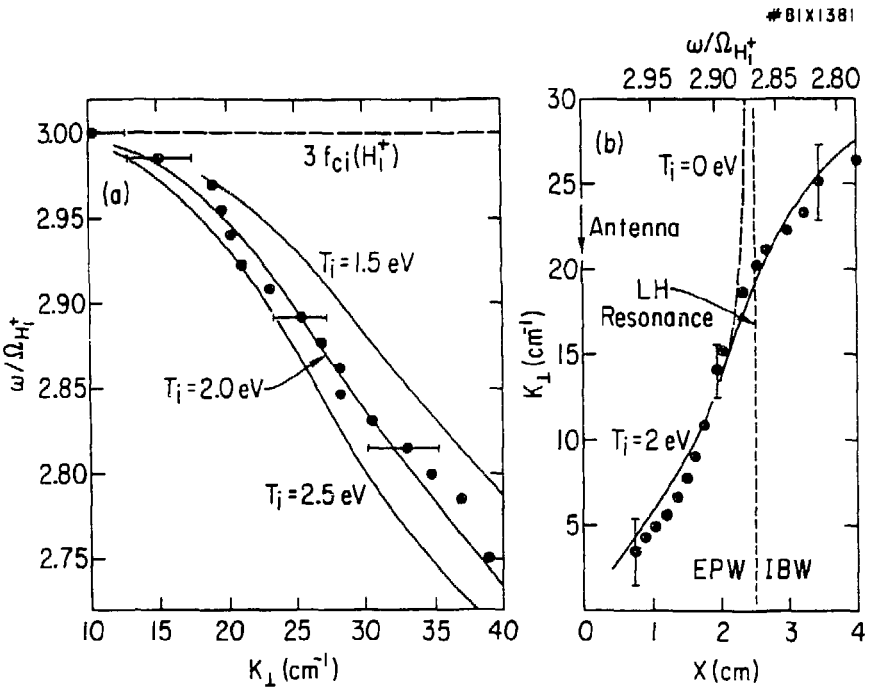
#81X1381
(a)
3 f_ci(H_1^+)
T_i = 1.5 eV
T_i = 2.0 eV
T_i = 2.5 eV
ω/Ω_H1+
K⊥ (cm⁻¹)
(b)
T_i = 0 eV
Antenna
LH
Resonance
T_i = 2 eV
EPW
IBW
X (cm)

Fig. 14

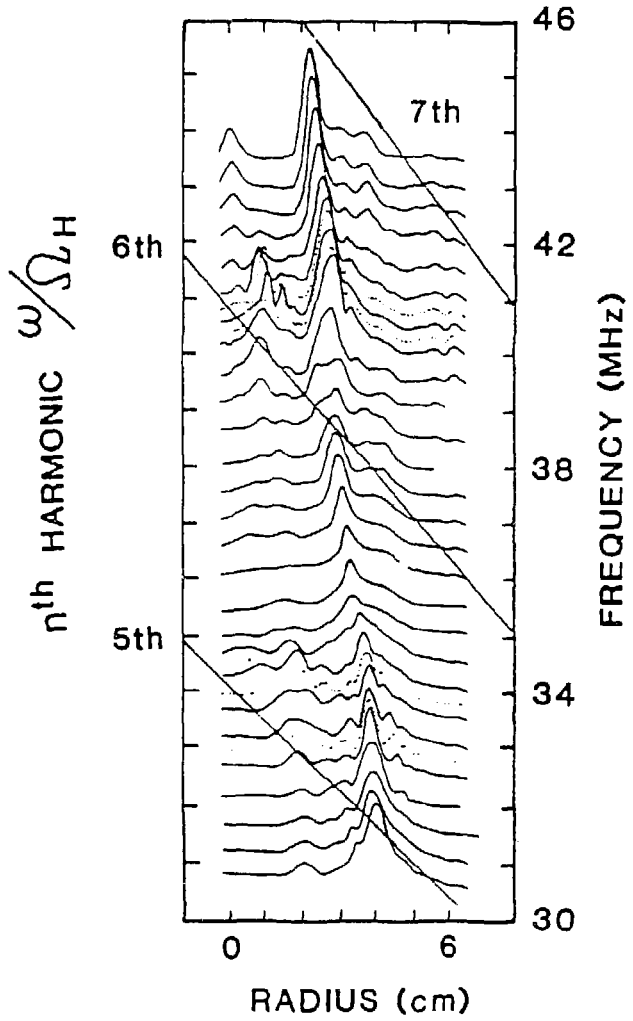
46
7th
6th
42
38
5th
34
30
0
6
RADIUS (cm)
FREQUENCY (MHz)
n^th HARMONIC ω/Ω_H

Fig. 15

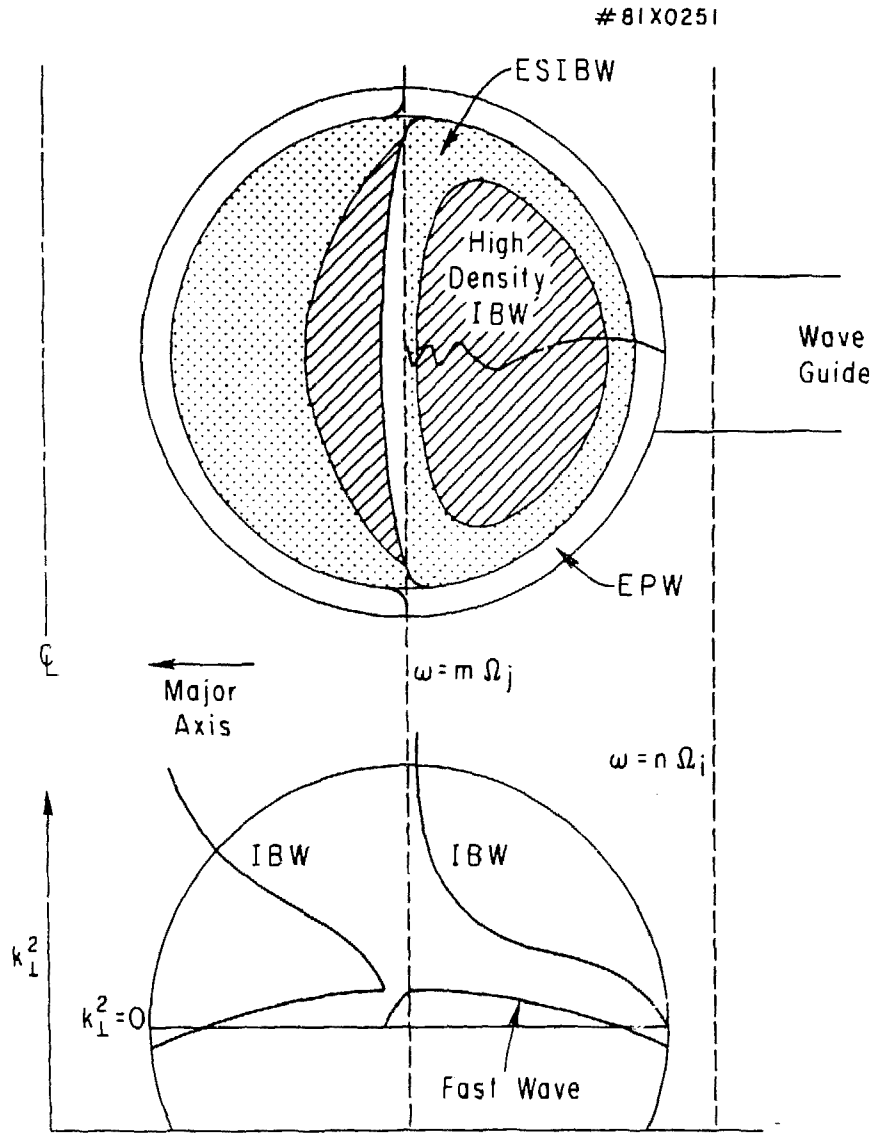
#81X0251
ESIBW
High
Density
IBW
Wave
Guide
EPW
℄
Major
Axis
ω = m Ω_j
ω = n Ω_i
IBW
IBW
k_⊥^2
k_⊥^2 = 0
Fast Wave

Fig. 16

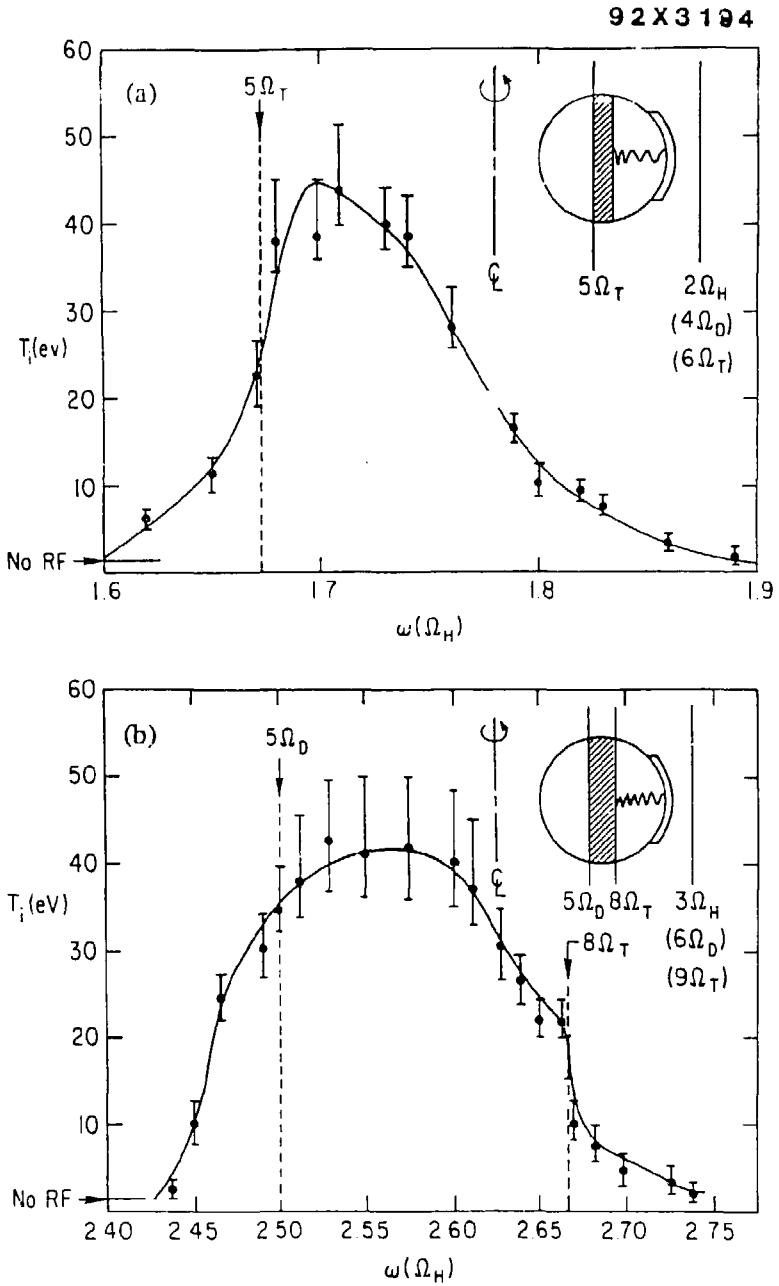
92X3194
(a)
5Ω_T
T_i(ev)
No RF
ω(Ω_H)
5Ω_T
2Ω_H
(4Ω_D)
(6Ω_T)
(b)
5Ω_D
T_i(eV)
No RF
ω(Ω_H)
5Ω_D 8Ω_T
8Ω_T
3Ω_H
(6Ω_D)
(9Ω_T)

Fig. 17

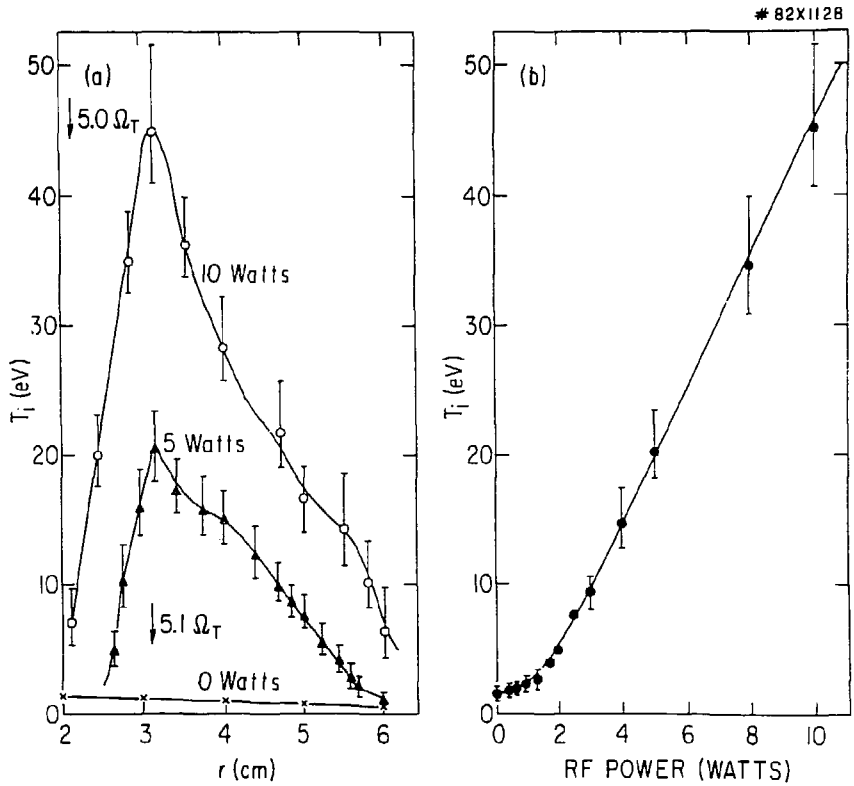
#82X1128
(a)
5.0 Ω_T
10 Watts
5 Watts
5.1 Ω_T
0 Watts
T_i (eV)
r (cm)
(b)
T_i (eV)
RF POWER (WATTS)

Fig. 18

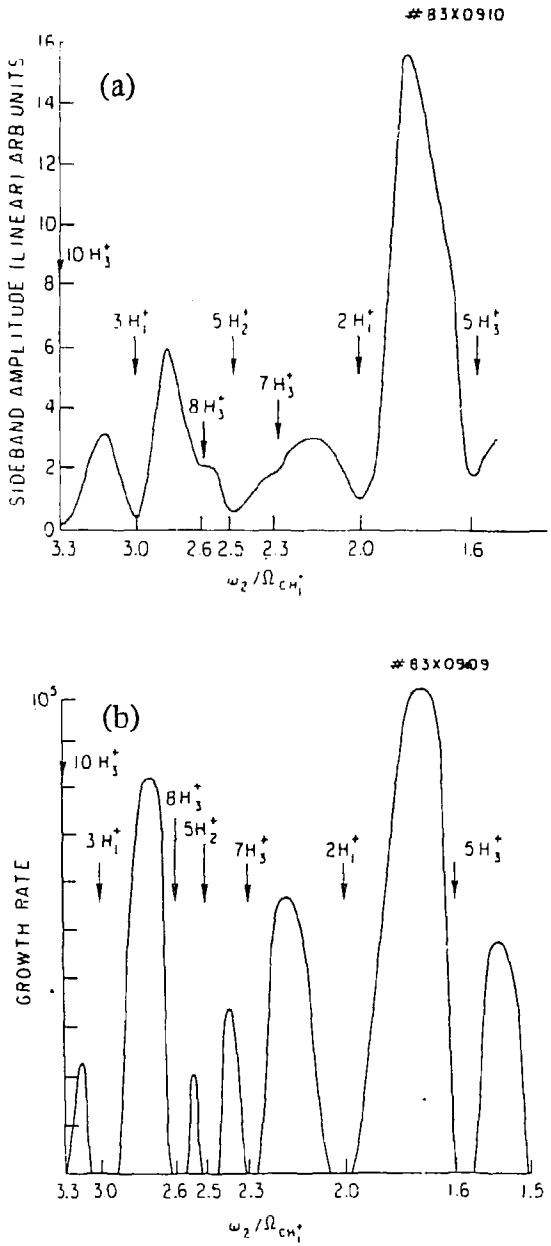
#83X0910
(a)
SIDEBAND AMPLITUDE (LINEAR) ARB UNITS
16
14
12
10
8
6
4
2
0
10 H$_3^+$
3 H$_1^+$
5 H$_2^+$
2 H$_1^+$
5 H$_3^+$
8 H$_3^+$
7 H$_3^+$
3.3
3.0
2.6
2.5
2.3
2.0
1.6
$\omega_2/\Omega_{cH_1^+}$
#83X0909
(b)
10^5
GROWTH RATE
10 H$_3^+$
8 H$_3^+$
3 H$_1^+$
5 H$_2^+$
7 H$_3^+$
2 H$_1^+$
5 H$_3^+$
3.3
3.0
2.6
2.5
2.3
2.0
1.6
1.5
$\omega_2/\Omega_{cH_1^+}$

Fig. 19

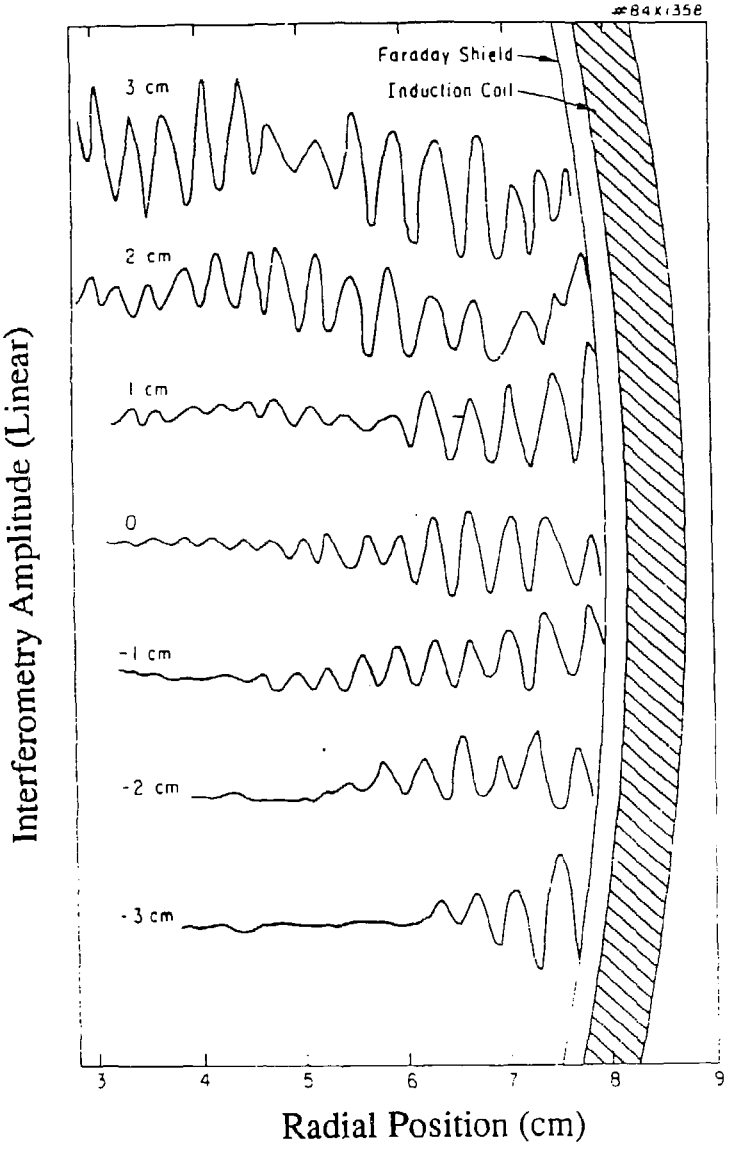
#84x135e
Faraday Shield
Induction Coil
3 cm
2 cm
1 cm
0
-1 cm
-2 cm
-3 cm
Interferometry Amplitude (Linear)
3
4
5
6
7
8
9
Radial Position (cm)

Fig. 20

EXTERNAL DISTRIBUTION IN ADDITION TO UC-420

Dr F. Paoloni, Univ. of Wollongong, AUSTRALIA
Prof. M.H. Brennan, Univ. of Sydney, AUSTRALIA
Plasma Research Lab., Australian Nat. Univ., AUSTRALIA
Prof. I.R. Jones, Flinders Univ, AUSTRALIA
Prof. F. Cap, Inst. for Theoretical Physics, AUSTRIA
Prof. M. Heindler, Institut für Theoretische Physik, AUSTRIA
Prof. M. Goossens, Astronomisch Instituut, BELGIUM
Ecole Royale Militaire, Lab. de Phy. Plasmas, BELGIUM
Commission-European, DG. XII-Fusion Prog., BELGIUM
Prof. R. Boucique, Rijksuniversiteit Gent, BELGIUM
Dr. P.H. Sakanaka, Instituto Fisica, BRAZIL
Instituto Nacional De Pesquisas Espaciais-INPE, BRAZIL
Documents Office, Atomic Energy of Canada Ltd., CANADA
Dr. M.P. Bachynski, MPB Technologies, Inc., CANADA
Dr. H.M. Skarsgard, Univ. of Saskatchewan, CANADA
Prof. J. Teichmann, Univ. of Montreal, CANADA
Prof. S.R. Sreenivasan, Univ. of Calgary, CANADA
Prof. T.W. Johnston, INRS-Energie, CANADA
Dr. R. Bolton, Centre canadien de fusion magnétique, CANADA
Dr. C.R. James,, Univ. of Alberta, CANADA
Dr. P. Lukác, Komenského Universzita, CZECHO-SLOVAKIA
The Librarian, Culham Laboratory, ENGLAND
Library, R61, Rutherford Appleton Laboratory, ENGLAND
Mrs. S.A. Hutchinson, JET Library, ENGLAND
Dr. S.C. Sharma, Univ. of South Pacific, FIJI ISLANDS
P. Mähönen, Univ. of Helsinki, FINLAND
Prof. M.N. Bussac, Ecole Polytechnique,, FRANCE
C. Mouttet, Lab. de Physique des Milieux Ionisés, FRANCE
J. Radet, CEN/CADARACHE - Bat 506, FRANCE
Prof. E. Economou, Univ. of Crete, GREECE
Ms. C. Rinni, Univ. of Ioannina, GREECE
Dr. T. Mual, Academy Bibliographic Ser., HONG KONG
Preprint Library, Hungarian Academy of Sci., HUNGARY
Dr. B. DasGupta, Saha Inst. of Nuclear Physics, INDIA
Dr. P. Kaw, Inst. for Plasma Research, INDIA
Dr. P. Rosenau, Israel Inst. of Technology, ISRAEL
Librarian, International Center for Theo. Physics, ITALY
Miss C. De Palo, Associazione EURATOM-ENEA , ITALY
Dr. G. Grosso, Istituto di Fisica del Plasma, ITALY
Prof. G. Rostangni, Istituto Gas Ionizzati Del Cnr, ITALY
Dr. H. Yamato, Toshiba Res. & Devel. Center, JAPAN
Prof. I. Kawakami, Hiroshima Univ., JAPAN
Prof. K. Nishikawa, Hiroshima Univ., JAPAN
Director, Japan Atomic Energy Research Inst., JAPAN
Prof. S. Itoh, Kyushu Univ., JAPAN
Research Info. Ctr., National Instit. for Fusion Science, JAPAN
Prof. S. Tanaka, Kyoto Univ., JAPAN
Library, Kyoto Univ., JAPAN
Prof. N. Inoue, Univ. of Tokyo, JAPAN
Secretary, Plasma Section, Electrotechnical Lab., JAPAN
S. Mori, Technical Advisor, JAERI, JAPAN
Dr. O. Mitarai, Kumamoto Inst. of Technology, JAPAN
J. Hyeon-Sook, Korea Atomic Energy Research Inst., KOREA
D.I. Choi, The Korea Adv. Inst. of Sci. & Tech., KOREA
Prof. B.S. Liley, Univ. of Waikato, NEW ZEALAND
Inst of Physics, Chinese Acad Sci PEOPLE'S REP. OF CHINA
Library, Inst. of Plasma Physics, PEOPLE'S REP. OF CHINA
Tsinghua Univ. Library, PEOPLE'S REPUBLIC OF CHINA
Z. Li, S.W. Inst. Physics, PEOPLE'S REPUBLIC OF CHINA
Prof. J.A.C. Cabral, Instituto Superior Tecnico, PORTUGAL
Dr. O. Petrus, AL. I. CUZA Univ., ROMANIA
Dr. J. de Villiers, Fusion Studies, AEC, S. AFRICA
Prof. M.A. Hellberg, Univ. of Natal, S. AFRICA
Prof. D.E. Kim, Pohang Inst. of Sci. & Tech., SO. KOREA
Prof. C.I.E.M.A.T, Fusion Division Library, SPAIN
Dr. L. Stenflo, Univ. of UMEA, SWEDEN
Library, Royal Inst. of Technology, SWEDEN
Prof. H. Wilhelmson, Chalmers Univ. of Tech., SWEDEN
Centre Phys. Des Plasmas, Ecole Polytech, SWITZERLAND
Bibliotheek, Inst. Voor Plasma-Fysica, THE NETHERLANDS
Asst. Prof. Dr. S. Cakir, Middle East Tech. Univ., TURKEY
Dr. V.A. Glukhikh,Sci. Res. Inst. Electrophys.I Apparatus, USSR
Dr. D.D. Ryutov, Siberian Branch of Academy of Sci., USSR
Dr. G.A. Eliseev, I.V. Kurchatov Inst., USSR
Librarian, The Ukr.SSR Academy of Sciences, USSR
Dr. L.M. Kovrizhnykh, Inst. of General Physics, USSR
Kernforschungsanlage GmbH, Zentralbibliothek, W. GERMANY
Bibliothek, Inst. Für Plasmaforschung, W. GERMANY
Prof. K. Schindler, Ruhr-Universität Bochum, W. GERMANY
Dr. F. Wagner, (ASDEX), Max-Planck-Institut, W. GERMANY
Librarian, Max-Planck-Institut, W. GERMANY
Prof. R.K. Janev, Inst. of Physics, YUGOSLAVIA